

# MaQuIs - Mars Quantum Gravity Mission

L. Wörner<sup>1</sup>, B. C. Root<sup>2</sup>, P. Bouyer<sup>3</sup>, C. Braxmaier<sup>1,4</sup>, D. Dirkx<sup>2</sup>, J. Encarnação<sup>2</sup>, E. Hauber<sup>5</sup>, H. Hussmann<sup>5</sup>, Ö. Karatekin<sup>6</sup>, A. Koch<sup>7</sup>, L. Kumanchik<sup>1</sup>, F. Migliaccio<sup>8</sup>, M. Reguzzoni<sup>8</sup>, B. Ritter<sup>6</sup>, M. Schilling<sup>7</sup>, C. Schubert<sup>7</sup>, C. Thieulot<sup>9</sup>, W. v. Klitzing<sup>10</sup>, O. Witasse<sup>11</sup>

<sup>1</sup>German Aerospace Center, Institute for Quantum Technologies, 89081 Ulm, Germany

<sup>2</sup>Delft University of Technology, Department of Space Engineering, Delft, the Netherlands

<sup>3</sup>Univ. of Amsterdam, Eindhoven Univ. of Technology, the Netherlands

<sup>4</sup>Universität Ulm University, Institute of Microelectronics, Albert-Einstein-Allee 43, 89081 Ulm, Germany

<sup>5</sup>German Aerospace Center, Institute of Planetary Research, 12489 Berlin, Germany

<sup>6</sup>Royal Observatory of Belgium, Brussels, Belgium

<sup>7</sup>German Aerospace Center, Institute for Satellite Geodesy and Inertial Sensing, Callinstrasse 30b, 30167 Hannover, Germany

<sup>8</sup>Politecnico di Milano, Department of Civil and Environmental Engineering, Milan, Italy

<sup>9</sup>Mantle dynamics group, Utrecht University, The Netherlands

<sup>10</sup>Institute for Electronic Structure and Laser, Foundation for Research and Technology Hellas, Heraklion, Greece

<sup>11</sup>European Space Agency, ESTEC, Noordwijk, The Netherlands

## Key Points:

- Mars
- Gravimetry
- Quantum Technologies

---

Corresponding author: Lisa Wörner, [lisa.woerner@dlr.de](mailto:lisa.woerner@dlr.de)

## Abstract

The aim of this paper is to propose a Mars Quantum Gravity Mission (MaQuIs). The mission is targeted at improving the data on the gravitational field of Mars, enabling studies on planetary dynamics, seasonal changes, and subsurface water reservoirs. MaQuIs follows well known mission scenarios, currently deployed for Earth, and includes state-of-the-art quantum technologies to enhance the gained scientific signal.

## Plain Text Summary

MaQuIs is a mission to map the gravity field of Mars to investigate subsurface structures and observe temporal changes. Consequently, MaQuIs yields information on the development of the planet and allows a deeper view into the structure and internal processes than ever before. For this purpose, MaQuIs deploys quantum mechanical systems to measure the gravity field following successful missions such as GRAIL and GRACE on the Moon and Earth respectively.

## 1 Introduction

The study of planets is interesting for several different reasons, such as planetary composition, evolution, and density, surface properties, prospecting, and comparative planetology (Glassmeier, 2020). One major subject of study is the search for water in planets outside Earth (Nazari-Sharabian et al., 2020; O'Rourke et al., 2020; Peddinti & McNamara, 2019; Bibring et al., 2006). Especially important in this case is the abundance of liquid water, since it could foster life and support a potential landing party.

In addition to static water distribution on a planet, shifts and dynamics in the planets density, are of high importance. The comparison to Earth's dynamics, allows to deepen the understanding of both the Earth's and the planets dynamics and consequently study phenomena such as climate change, seismic activity, seasonal variations, or volcanic eruptions. With those data available, inner structures can be modelled and predictions made (Banerdt et al., 2020).

For this purpose different missions, orbiting planets, landing on planets and comets, and samples return missions, have been carried out in the past.

Here, we propose a Mars Quantum Gravity Mission, MaQuIs, which aims at improving the current knowledge of the gravitational field map of Mars and thereby enabling research of seasonal changes, planetary dynamics, and subsurface water occurrences.

49 Similar to Earth and Lunar satellite gravimetry missions, static occurrences, marked by differences  
50 in density as well as dynamical processes are detectable from orbit. Such a dedicated gravity mission would  
51 improve the static gravitational field model of Mars, determine its temporal components, and allow to  
52 pinpoint the distribution of water with a higher accuracy than current orbital missions. Additionally, a  
53 more detailed knowledge of the gravitational field distribution paves the way to improving not only the  
54 depth resolution of subsurface lakes and their distribution around the entire planet, but also to identify  
55 and characterise other buried mass structures like hidden impact craters (Frey et al., 2002) and magma  
56 chambers (Mari et al., 2020; Broquet & Andrews-Hanna, 2022).

57 Recently, missions have been proposed for low Mars orbit to improve existing geodetic and remote  
58 sensing data-sets using current techniques of gravity field determination and orbit determination based  
59 on Doppler tracking and inter-satellite radio links (Genova, 2020; Oberst et al., 2022). Landers can sup-  
60 port such global missions, as their resolution for a specific area is increased on the expense of being re-  
61 stricted to a limited area.

62 A dedicated global gravity mission would allow to identify interesting sites for further robotic ground  
63 based investigation, including possible drilling sites and to prepare human exploration with identifica-  
64 tion of potential landing sites with local sources for In-Situ Resource Utilisation (ISRU).

65 MaQuIs will follow the mission design of GRACE (Tapley et al., 2004), GRICE (Lévêque et al., 2021),  
66 CARIOQA (Lévêque et al., 2022), and GRAIL (Zuber et al., 2013). MaQuIs will deploy quantum me-  
67 chanical systems to enable the gravity field measurement. This increases the resolution of the gravita-  
68 tional field map, as discussed for similar missions for Earth (Carraz et al., 2014; Lévêque et al., 2021, 2022).  
69 Additional optomechanical sensors and optical link technologies enable the proposed mission. In the fol-  
70 lowing, the mission is outlined, giving an overview over scientific goals, system level requirements, an en-  
71 visioned mission design, and orbital considerations.

## 72 **2 Scientific Goals**

73 Gravitational data can be used to study the surface and subsurface of the planet leading to improved  
74 understanding of the Martian crust and lithosphere (Beuthe et al., 2012). Such data also holds the po-  
75 tential to investigate dynamic surface processes, such as atmospheric seasonal changes, appearance of ice  
76 sheets, and large scale erosion of the Martian surface.

77 While dynamic surface effects can be observed by optical means, such as spectroscopy and imagery,  
 78 subsurface effects and density distributions require additional instruments. With seismographs and ra-  
 79 diography being two deployed possibilities, the study of the gravitational field supported by information  
 80 on the visible shape of the planet enables the study of static and dynamic processes under the planet's  
 81 surface. The accuracy of both information, the imagery and the gravitational field data, determine the  
 82 accuracy of predictions and the quality of models of the internal structure and planetary composition.  
 83 Additionally, sufficiently accurate measurements allow the identification of areas of high or low mass den-  
 84 sity and their dynamics, leading to the identification of interesting regions and determination of future  
 85 landing sites.

## 86 2.1 Gravity Maps of Mars

87 Over the past decade, Mars has taken more and more of the spotlight. Several missions to inves-  
 88 tigate local and global properties of the Red Planet have been successfully operated, one of the latest be-  
 89 ing Perseverance (Jacobstein, 2021). Future planned missions to Mars and its moons include orbiters and  
 90 landers (Muirhead et al., 2020). Consequently, Mars is already orbited by several different satellites.

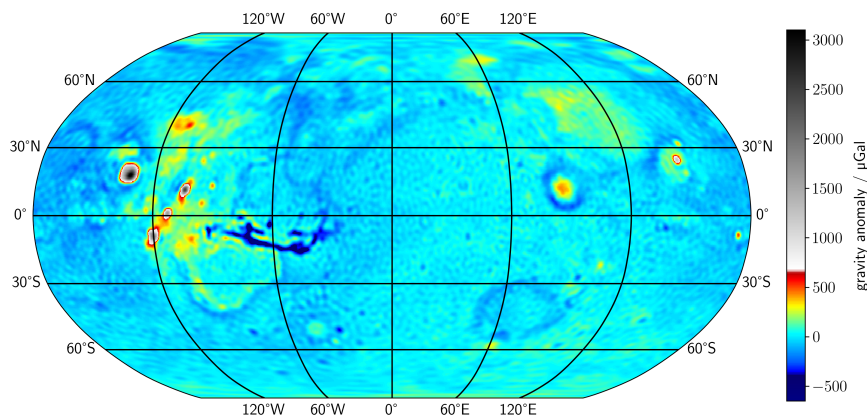


Fig. 1: Gravity anomaly of Mars from MRO120F (Konopliv et al., 2020).

91 From orbits determined by Doppler tracking observations, the current resolution of the gravitational  
 92 field map of Mars is in the order of 115 km at ground level (Konopliv et al., 2011, 2016; Genova et al.,  
 93 2016). Figure 1 shows the gravity anomalies on the areoid, the planetary geoid of Mars, up to degree and

94 order 120. A large correlation of the field is seen with the small scale topography. The dichotomy observed  
 95 in the topography of Mars is missing in the gravity anomalies, suggesting some form of local isostasy in  
 96 the sub-surface. Another global gravity feature stands out, related to the volcanic region, the Tharsis Rise.  
 97 A large positive gravity anomaly (approximate 300 mGal) situated at the Tharsis Rise is surrounded by  
 98 a ring of negative gravity anomaly (approximate  $-300$  mGal), seemingly detached from any geologic fea-  
 99 ture. A feature that also stands out in the degree and order (d/o) 2-3 of the spherical harmonic coeffi-  
 100 cients that capture the spectral content of the gravitational field.

101 Figure 2 shows the degree variances (or spectral signatures) of several Martian gravity field mod-  
 102 els with its uncertainty estimates. We compare here the four most used versions of the Martian gravi-  
 103 tational field: GGMRO-95 (Konopliv et al., 2006), GMM-3-120 (Genova et al., 2016), JGMRO-120d (Konopliv  
 104 et al., 2016), and JGMRO-120F models (Konopliv et al., 2020)). All four fields coincide up to degree and  
 105 order 60, where the oldest model GGMRO-95 starts to divert. The newer models include more and lower  
 106 orbital data improving the resolution and accuracy of the model. The dashed lines denote the error es-  
 107 timates of these models. Around degree 100 the error estimates cross the actual model content, which  
 108 shows that the models can only be thrust up to degree 100, which stands for a spatial resolution of 115  
 109 km.

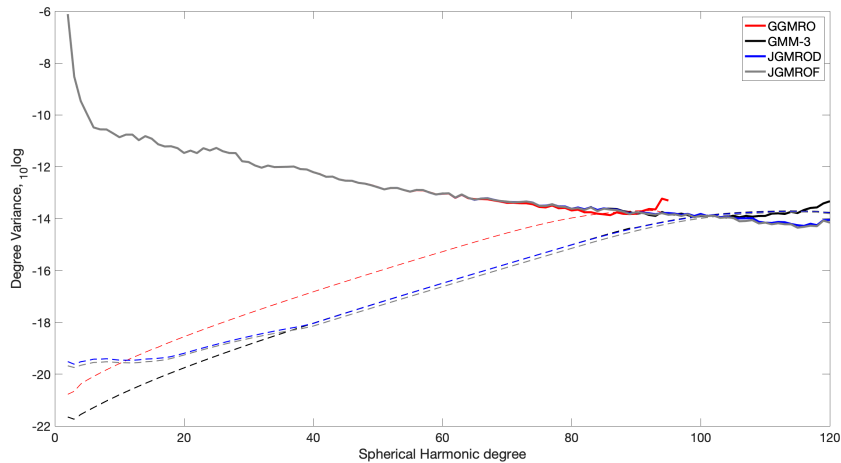


Fig. 2: Spectral signature of several Mars gravity models found on NASA's Planetary Data System (GGMRO-95 (Konopliv et al., 2006), GMM-3-120 (Genova et al., 2016), JGMRO-120d (Konopliv et al., 2016), and JGMRO-120F models (Konopliv et al., 2020)).

110 The observed orbits used to construct these gravitational models need to be corrected for non-conservative  
111 accelerations acting on the satellite, like atmospheric drag and solar radiation pressure, prior to or dur-  
112 ing gravity field recovery (Konopliv et al., 2006). Incorrect modelling of these effects will leak into the  
113 gravity field models as clearly shown by the improved consistency in results obtained by Genova et al.  
114 (2016) after incorporating a more detailed atmosphere model. A dedicated gravity field mission will not  
115 only result in an improved gravity field model of Mars, but also give insights in better atmospheric mod-  
116 els of Mars (Doornbos, 2012), which is in turn important for interpreting temporal gravity signatures (Petricca  
117 et al., 2022).

## 118 **2.2 Water on Mars**

### 119 ***2.2.1 Liquid Water on Mars***

120 Abundant morphological and mineralogical evidence points to large amounts of liquid water that  
121 must have been present at the surface of early Mars (Carr & Head, 2015; Bibring et al., 2006). Large parts  
122 of that early reservoir have been lost to space (Jakosky, 2021), and today, the largest known part of the  
123 remaining martian water is present in the polar caps (Byrne, 2009), in near-surface ice deposits in high  
124 and mid-latitudes (Holt et al., 2008; Dundas et al., 2021), and as water in hydrated minerals (Carter et  
125 al., 2023). However, it cannot be excluded that liquid water is present even today in the subsurface in  
126 the form of deep groundwater (Grimm et al., 2017) underlying a thickening cryosphere (Clifford et al.,  
127 2010). In fact, radar measurements suggest that a briny layer of liquid water may exist beneath a 1.5 km-  
128 thick part of the south polar ice cap (Lauro et al., 2021), however, this interpretation of the data is de-  
129 bated (I. B. Smith et al., 2021; Bierson et al., 2021). If there are any aquifers now, the depths to the ground-  
130 water table are thought to be 2-7 km in equatorial zone and 11-20 km at the poles (Stamenkovic et al.,  
131 2021). The contrast of the lighter density of such aquifers, if present, with respect to the heavier Mar-  
132 tian basaltic crust makes the MaQuIs gravity mission ideal for detecting and exploring locations and size  
133 of possible present-day aquifers or the permeable structures that host them (porous sediments, fractured  
134 basalts). The mission could also detect how seasonal and orbital changes of Mars affect the groundwa-  
135 ter level on Mars. High precision gravity observations could explore this subsurface phenomenon, which  
136 would have important implications for the current habitability of Mars.

### 2.2.2 Volatile-rich Subsurface Sediments on Mars

One main objective of the proposed mission is the identification and quantification of volatile-rich sediment reservoirs. Numerous landforms on Mars have been interpreted as mud volcanoes and corresponding mud flows, i.e. the results of subsurface sediment mobilization and subsequent ascent, eruption and surface emplacement of volatile-rich, liquefied sediments (Skinner & Tanaka, 2007; Oehler & Allen, 2010; Komatsu et al., 2016; Brož et al., 2019; Orgel et al., 2019; Cuřín et al., 2023). Such deposits are prime targets for geological research, as they bear a record of aqueous processes at depth and are not heavily affected by high-temperature and high-pressure alteration (unlike impact ejecta). As such, they enable access to materials that were formed in the early history of Mars. Moreover, mud volcanoes would be promising sites to search for biosignatures, as mud volcanoes on Earth are known to be habitats for thriving bacterial communities (Fryer et al., 2020) and, by analogy, may have provided suitable conditions for life on Mars (Oehler et al., 2021). However, the interpretation of landforms is typically not unambiguous, and at least part of the hypothesized mud volcanoes may also have been formed as 'true', igneous volcanoes. It is therefore essential to test the mud volcano hypothesis by identifying subsurface reservoirs of volatile-rich sediments. On Earth, mud volcanoes are typically associated with density anomalies (Nettleton, 1979; Doo et al., 2015), and gravity surveys are routinely used to characterize sedimentary basins which typically display negative gravity anomalies (Bott, 1960). The contrast between less dense sediments and the denser basaltic and other magmatic rocks that constitute the bulk of the crust will enable MaQuIs to identify sediment subsurface reservoirs and quantify their masses. A comparison of derived gravity maps with the distribution of possible mud volcanoes will inform our search for deep volatiles and possible habitable subsurface niches on Mars ('deep biosphere', e.g. Michalski et al., 2013).

### 2.3 Temporal gravity changes and seasonal behavior of CO<sub>2</sub> ice

The climate of planets are subject to changes in time due to several causes including astronomical forcing (variations of orbital elements), atmospheric escape or out-gassing following natural events. The stability of present day Mars climate and the secular changes are crucial to understand its long term dynamics (Haberle & Kahre, 2010). Analysis has shown that Mars possibly once harboured liquid water on the surface and had a denser atmosphere (Nazari-Sharabian et al., 2020). This combination renders it possible that there once were life forms roaming its surface. Those factors allow to infer a climate collapse taking place in Mars' history. Understanding the processes that led to that event and the still on-

166 going seasonal changes including the appearance of surface carbon-dioxide ice, render Mars a relevant sub-  
167 ject to predicting Earth's future. To gain a complete picture of the underlying processes, internal as well  
168 as surface structures and deposition dynamics are important to study.

169 In addition, the dynamics of the Martian surface, especially with respect to the seasonal sublima-  
170 tion and deposition of Mars atmospheric carbon-dioxide, should be studied intensely as that will give in-  
171 sight in the viscosity structure of the mantle. Mars is continuously subjected to surface loading induced  
172 by seasonal mass changes in the atmosphere and ice caps due to the CO<sub>2</sub> sublimation and condensation  
173 process. It results in surface deformations and in time variations of gravity.

174 Time variations of gravity are not only due to mass variations in surface fluid layers but also to sur-  
175 face loading deformations of the solid component of the planet induced by them (Karatekin et al., 2011).  
176 With about one third of Mars' atmosphere being deposited and sublimated in those seasonal changes,  
177 the impact on its gravitational field and rotation are immediately recognizable (Karatekin, Van Hoolst,  
178 Tastet, et al., 2006). The deformations of the planet depend on its internal structure, particularly on its  
179 density and elastic parameters. The effect of the internal structure of Mars on its loading deformation  
180 is determined via Mars' load Love numbers which depend strongly on the mean radial structure. Low de-  
181 gree load Love numbers (inferior to degree 10) depend essentially on the radius of the core and on its rhe-  
182 ological properties (Métivier et al., 2008). While the effect has been observed (Konopliv et al., 2011), the  
183 dynamics itself and the driving forces are still subject to active research. More precise gravitational field  
184 data can aid in the research of these dynamics.

185 The carbon-dioxide results in permanent ice sheets of a thickness of approximately 2 km and areas  
186 with a diameter of roughly 1000 km and 400 km on the Northern and Southern polar caps respectively.  
187 The deposited ice sheet is far from smooth and includes steep cliffs and troughs. While some of those pat-  
188 terns can be attributed to rotation, Coriolis forces, and winds, the models currently fall short in explain-  
189 ing all observations. Moreover, precise gravitational field data could shed light on subterranean struc-  
190 tures and density distributions, aiding in building more complete models of the polar ice sheets, explain-  
191 ing the occurring shapes.

192 The largest signature in the seasonal mass exchange between the Mars polar caps is given by vari-  
193 ations in the zonal coefficient of Mars. Martian degree 2 and 3 time-variable gravity coefficients have been  
194 estimated by different authors using Mars orbiter radio tracking data (e.g. Konopliv et al., 2011; Gen-  
195 ova et al., 2016) as well as numerical general circulation models (Karatekin et al., 2005). The seasonal time

196 variations of gravity are expected to be mostly induced by surface fluid dynamics as show by high cor-  
 197 relations of these observations with atmospheric models (Karatekin, Van Hoolst, & Dehant, 2006)

198 Sensitivity studies of the orbital tracking based gravity models show that some seasonal gravity sig-  
 199 nature can be absorbed in the drag model if constraint is too loose (Konopliv et al., 2011). This shows  
 200 that a dedicated gravity mission would not only result in a more accurate determination of the tempo-  
 201 ral gravity field, but would also improve atmospheric models of Mars. The  $J_3$  changes are larger and bet-  
 202 ter detectable than the  $J_2$  temporal variations, on average the odd degrees are about 20 percent higher  
 203 than the even degrees (Konopliv et al., 2011). This signal is linked to the seasonal CO<sub>2</sub> ice mass exchange  
 204 of the northern and southern poles of Mars (Konopliv et al., 2011). This mass exchange between poles  
 205 is estimated to be  $\pm 4 \times 10^{15}$  kg and consistent between different studies (Konopliv et al., 2006; Smith,  
 206 2009; Yoder et al., 2003). More recent, seasonal variation of the  $J_2$ ,  $J_3$ ,  $J_4$ , and  $J_5$  coefficients have been  
 207 estimated from orbital tracking (Genova et al., 2016) and show similar trends in the polar mass exchange.  
 208 The Mars Orbiter Laser Altimeter (MOLA) on the Mars Global Surveyor (MGS) spacecraft, measured  
 209 seasonal changes in the ice thickness up to 1.5 - 2 meters due to the carbon dioxide cycle (D. E. Smith  
 210 et al., 2001). The volume of CO<sub>2</sub> and water ice variability is estimated to be  $9.4 \times 10^{12}$  m<sup>3</sup> to  $9.6 \times 10^{12}$  m<sup>3</sup>  
 211 for the Southern and Northern polar caps based on MOLA measurements (Xiao, Stark, Schmidt, Hao,  
 212 Steinbrügge, et al., 2022; Xiao, Stark, Schmidt, Hao, Su, et al., 2022). .

213 In addition to atmospheric mass transport, tidal deformation of Mars also results in a time-variable  
 214 gravity signal. Although this signature is substantially larger than that of the atmospheric mass trans-  
 215 port, its behaviour is much more predictable and easily quantified. Typically, its influence is parameter-  
 216 ized by the  $k_2$  Love number that quantifies time-variability of the degree-two gravity field coefficients.  
 217 This Love number is an important independent geodesy constraint (Rivoldini et al., 2011), and helps to  
 218 constrain the rigidity structure and core size of Mars (Pou et al., 2022). It has been determined in var-  
 219 ious previous Mars gravity field determinations (Konopliv et al., 2011, 2016; Genova et al., 2016), where  
 220 (Genova et al., 2016) shows the strong need for proper modelling of the atmospheric properties to prop-  
 221 erly extract the signature of the Love number. For the Moon, separate values of  $k_{20}$ ,  $k_{21}$  and  $k_{22}$  have  
 222 been determined using GRAIL data, providing further interior constraints (Williams et al., 2014). Al-  
 223 though these values of  $k_{2m}$  at different orders  $m$  proved to be almost equal to one another, their small  
 224 differences may be relevant in processing of high-accuracy data proposed here. Past attempts to mea-  
 225 sure these separate coefficients using Doppler tracking proved unsuccessful for Mars. In addition to the

226 nominal value of the Love number(s), the phase lag of the tidal deformation, often quantified by the  $k_2/Q$   
227 value provides constraints on the Martian interior (Pou et al., 2022), and is a crucial parameter for the  
228 long-term orbital evolution of the Martian moons (Efroimsky & Lainey, 2007). At present, the Martian  
229  $k_2/Q$  at Phobos' forcing frequency is best constraint by the secular acceleration of Phobos' orbit, as de-  
230 termined in its ephemeris (Lainey et al., 2021). Determining the frequency-dependence of  $k_2/Q$  could pro-  
231 vide further constraints on both Mars interior and system evolution, provided their signature in the data  
232 could be decoupled (Dirkx et al., 2014).

233 Studying the formation of the Tharsis Rise will reveal more information about the planet's interior  
234 and its thermal evolution. One big question to solve is if the mantle underneath the Tharsis Rise is still  
235 active and taking part in dynamically upholding the volcanic dome. The Insight mission is placed near  
236 Elysium Mons, which is in the seismographic shadow zone of the Tharsis Rise and therefore receives less  
237 information from that area. However, a dedicated gravimetry mission that would be capable of measur-  
238 ing gravity-rate data could observe if there are changes in the gravity field due to mantle flow. A sim-  
239 ilar phenomenon on Earth, yet due to another physical process, is observed by GRACE: mantle flow due  
240 to Glacial Isostatic Adjustment (Steffen et al., 2009; Root et al., 2016). A prominent feature in the free-  
241 air anomaly and in the isostatic anomaly of Mars is a huge gravity signal at the Tharsis Rise with an ex-  
242 treme high at the center of the dome, surrounded by a negative ring around the region (Zhong & Roberts,  
243 2003). Because it is also visible in the isostatic anomaly it could be interpreted as still active readjust-  
244 ment (Root et al., 2015), meaning mantle plume movement underneath the Tharsis Dome. A prelimi-  
245 nary study (Root et al., 2022) of a mantle anomaly underneath the volcanic region, suggests 12  $\mu\text{Gal}/\text{yr}$   
246 gravity change for the very long wavelength gravity signal. This will require accurate observations of the  
247 secular change of the gravity field, decoupled from any atmospheric interactions.

## 248 **2.4 Internal Structure and Composition of Mars**

249 The internal structure of any planetary body, including tectonic lithosphere, core size, mass distri-  
250 bution, and material composition, are an intensely studied field to understand the formation of planets  
251 and their current dynamics. This includes phenomena such as volcanic and seismologic activities. To study  
252 those on Mars, a seismograph was deployed on Mars' surface (Lognonné et al., 2019) with the Insight mis-  
253 sion. By studying the seismographic data from the Insight mission, new insights were obtained into the  
254 inner composition and structure of the planet and they have given new constraints in lithospheric and

255 mantle dynamic modelling. Based on determination of the polar moment of inertia, the tidal varying po-  
256 tential and seismic data from the Insight mission the Martian core radius was determined as  $1830\pm 40$  km  
257 (Stähler et al., 2021). The corresponding core density ranges between  $5800\text{ kg/m}^3$  to  $6200\text{ kg/m}^3$  show-  
258 ing substantial amounts of volatiles contained in the core when compared to a pure iron density of about  
259  $8000\text{ kg/m}^3$ . From the lack of S-waves in the seismic record a fluid state of the core is derived. At the  
260 Insight landing site a crustal thickness of  $39\pm 8$  km was derived from seismic data (Knapmeyer-Endrun  
261 et al., 2021) which fits to global estimates of crustal thickness from gravity and topography data of 27 km  
262 to 89 km (Neumann et al., 2004). The expected crustal thickness variations depend on the assumed struc-  
263 ture with possibilities of (a) a homogeneous crustal density, (b) an upper porous layer and more compact  
264 material in the lower part of the crust and (c) a possible dichotomy between northern and southern part  
265 of the crust (Wieczorek et al., 2022). Complementary to seismic data, the gravitational field distribution  
266 can be used to improve our understanding of the inner structure. With the current gravity field models  
267 obtained by tracking the orbital spacecraft, the global resolution of the Martian gravity fields is known  
268 up to wavelengths of approximately 115 km (90 d/o) (Konopliv et al., 2011; Genova et al., 2016). Due  
269 to the elliptical orbits of the tracked spacecraft there remain asymmetries in the resolution of the grav-  
270 ity field with respect to northern and southern latitudes.

271 The gravitational field distribution can be used to derive better understanding of the inner struc-  
272 ture. With the current gravity field models obtained by tracking the orbital spacecraft, the global res-  
273 olution of the Martian gravity fields is known up to wavelengths of approximately 115 km (90 d/o) (Konopliv  
274 et al., 2011).

275 On Mars two global surface features stand out that are a result of the internal dynamics of Mars:  
276 the crustal dichotomy and the Tharsis Rise, a huge volcanic province harbouring the largest volcano in  
277 the Solar system. Both structures are heavily debated about the time of formation, but the mechanism  
278 of formation is usually described by mantle plume volcanism (Zhong et al., 2007). A huge up welling pen-  
279 etrated the primarily crust during the Early Noachian depositing the rock mass that are now the south-  
280 ern highlands. Then, in the Late Noachian another plume eruption is responsible for the creation of the  
281 Tharsis Rise. This early creation of the Tharsis Rise is now debated (Bouley et al., 2016), because a later  
282 formation could have caused sufficient polar wander to explain the orientation of Noachian/Early Hes-  
283 perian valley networks around the equator, suggesting a different orientation of Mars in more humid cli-  
284 mate. Even the northern plains in this model lacks the heavily cratered landscape that would prove its  
285 old age. The northern plains are quite smooth and show less signs of heavy cratering. However, the old

286 surface could have been overprinted as a number of buried impact basins, called Quasi-Circular Depres-  
287 sions (QCD), were discovered that indicate the old age of the northern region (Frey et al., 2002). These  
288 QCDs are visible in the Mars Orbiter Laser Altimeter data, but do not have an imagery signature. High-  
289 resolution gravity observations could confirm the presence of buried impact structures.

290 Combining topographic (Klimczak et al., 2018) and gravity data (Zuber et al., 2000; Beuthe et al.,  
291 2012; Goossens et al., 2017) it is possible to study the structure of the martian lithosphere. Flexure the-  
292 ory (Watts & Burov, 2003) is able to compute characteristics of the lithosphere by studying the spectral  
293 interplay between topography and gravity. For example, Phillips et al. (2001) show that flexural litho-  
294 sphere loading is the main support of Tharsis for example, following the initial studies by Turcotte et al.  
295 (1981). A long standing research has been performed to estimate the elastic thickness on Mars, which  
296 controls the amount of support of which the lithosphere is capable, which is extreme on Mars. The Thar-  
297 sis region, one of the largest volcanic complexes in the Solar system, has been thoroughly studied (Belleguic  
298 et al., 2005; Beuthe et al., 2012; Lowry & Zhong, 2003; McKenzie et al., 2002). One drawback of this the-  
299 ory is buried mass anomalies that do not have any topographical signature (McKenzie et al., 2002). In-  
300 spection of the Bouguer anomaly of the Northern Hemisphere of Mars shows clear evidence of numer-  
301 ous sub-surface mass structures (Zuber et al., 2000). These structures are not only subsurface aquifers,  
302 but the northern hemisphere has many buried impact craters (QCD) that are indications of an Early-  
303 Noachian age, maybe going back to the primordial crust, now overprinted by southern erosion deposits  
304 (Frey et al., 2002). A recent flexure study by Root and Qin (2022) shows higher global density, confirm-  
305 ing high basaltic crust. Thin shell flexure is able to explain part of the long-wavelength features, but dy-  
306 namic flow is needed, and high lateral densities are present in the martian crust, as homogeneous mod-  
307 els cannot represent the gravity field completely. The need for lateral varying crustal density observa-  
308 tions is needed to better understand the geological past of Mars and its current state.

309 With gravity alone, it is difficult to determine the depth of these structures, whether they are present  
310 in the crust of upper mantle. Earth-based gravimetric studies (Bouman et al., 2013; Root et al., 2021)  
311 show that gravity gradients are more sensitive to crustal mass anomalies and are better capable of de-  
312 coupling them from any upper mantle mass anomalies. Global inversion modelling together with state-  
313 of-the-art flexural modelling show promising results in determining crustal and upper mantle mass anoma-  
314 lies, when using gravity gradient data (van Brummen, 2022). Global coverage of the gravitational field  
315 measurement allows for modelling of the entire planet and enable the study of large scale dynamics and

316 high mass erosion or deposition. Additionally, global data supplemented by local data and imagery can  
317 improve models and allow more precise predictions of local static and dynamical behavior. The latter is  
318 especially important to identify specific regions that show distinct different variations in the density struc-  
319 tures of the crust.

320 Image and topography (MOLA) data has to be combined with the gravitational field data to com-  
321 plete the picture of Mars surface and subsurface composition. With the abundance of images taken of  
322 Mars, MaQuIs will supply the necessary gravitational field data, leading to a global estimation of den-  
323 sity profiles and ground composition of Mars.

## 324 **2.5 Scientific Requirements**

325 For this scientific overview we identified the following requirements for a dedicated gravity field mis-  
326 sion to Mars.

- 327 • Spatial resolution: The resolution of the gravitational field shall be improved above the spherical  
328 harmonic (SH) degree 90 (approximately 115 km) for better flexural modelling of the Martian Litho-  
329 sphere.
- 330 • Minimum size aquifers: Mapping the crater size aquifers requires a resolution of 2880 degree and  
331 order spherical harmonic coefficients to detect. The Lunar gravity field's best resolution is in the  
332 order of 1200 d/o (Lemoine et al., 2013). As it is discussed, the Martian system already greatly  
333 benefits from an improvement of the current resolution which is up to the order of 90 - 100 degree  
334 and order. Larger aquifer volumes, such as that which created the Valley Marineris, can be mapped  
335 with a gravity field up to 360 degree and order.
- 336 • Quasi-Circular Depression (QCD) determination: MaQuIs shall improve the understanding of the  
337 formation of the dichotomy of Mars by determining the age of the northern hemisphere (Frey et  
338 al., 2002). If the QCD are identified as craters, this could change the age determination (by crater  
339 counting) of the northern hemisphere significantly.
- 340 • Global Coverage: Polar regions (ice sheets) are situated poleward above 80° latitude north and be-  
341 low 80° latitude south. MaQuIs shall cover that range to support glacial isostatic adjustment and  
342 Martian climate studies. This results in a requirement for a nearly polar orbit.

- 343 • Temporal frequency seasonal: The sub-yearly signal in  $C_{30} = \pm 5 \times 10^{-9}$  and  $C_{50} = \pm 3 \times 10^{-9}$   
 344 (Smith, 2009). The corresponding mass changes are in the north pole  $2 \pm 2 \times 10^{15}$  kg, south pole  
 345  $3 \pm 4 \times 10^{15}$  kg, atmosphere  $-4 \pm 2 \times 10^{15}$  kg respectively. MaQuIs shall be able to address these  
 346 changes.
- 347 • Temporal secular: Based on preliminary modeling mantle convection underneath the Tharsis re-  
 348 gion could come up to  $12 \mu\text{Gal}/\text{yr}$  (Root et al., 2022). As such, the secular drift in the Odyssey  $\bar{J}_3$   
 349 data is limited to  $0.9 \pm 0.9 \times 10^{-11}/\text{yr}$  (Konopliv et al., 2011). The gravitational data contains  
 350 this convection. MaQuIs aims at measuring its effects.

## 351 2.6 Proposed Mission

352 Figure 3, outlines the overall scheme of the measurement principle. The MaQuIs mission consists  
 353 of two satellites chasing one another along the orbit to map the gravitational field of Mars.

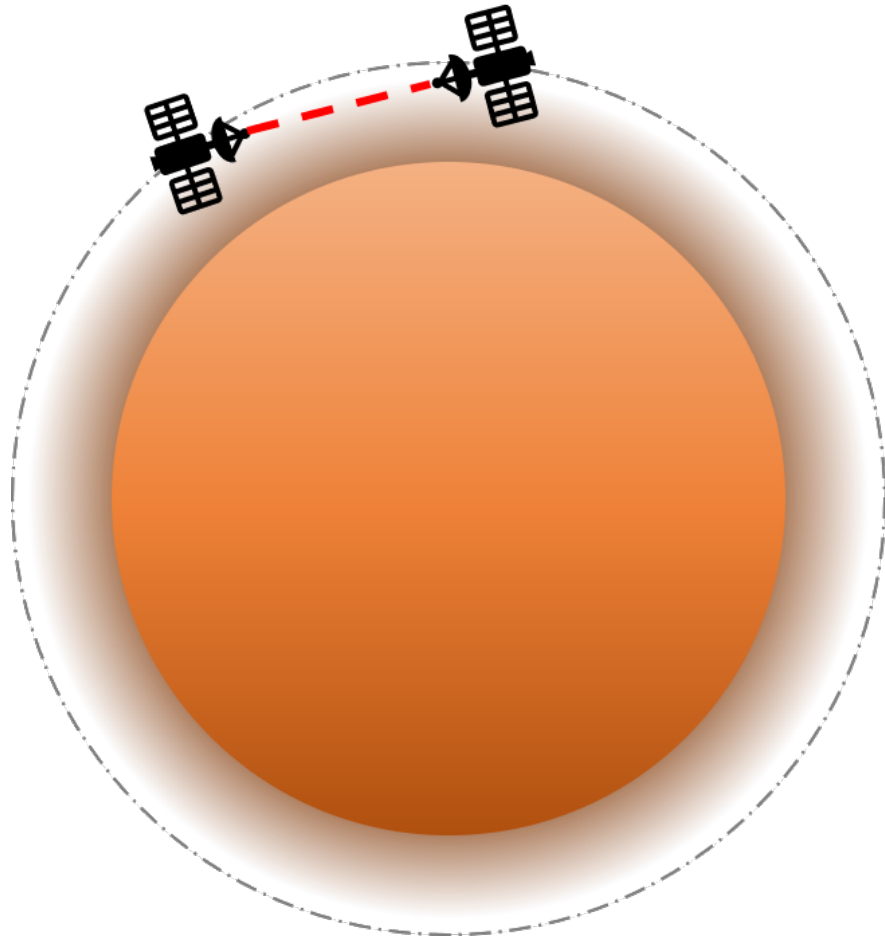


Fig. 3: A sketch to show the measurement principle: Two satellites chasing one-another along the same orbit to measure changes in the gravitational field by detecting the change in the distance between the satellites.

354 MaQuIs follows missions such as the Gravity field and steady-state Ocean Circulation Explorer (GOCE,  
 355 Rummel et al., 2011), the Gravity Recovery And Climate Experiment and its Follow-On mission (GRACE  
 356 and GRACE-FO, Tapley et al., 2004; Kayali et al., 2017), designed to detect static and dynamical pro-  
 357 cesses on Earth, as well as the Gravity Recovery and Interior Laboratory (GRAIL, Zuber et al., 2013)),  
 358 a GRACE like mission orbiting the Moon. Those missions, have successfully demonstrated that the out-  
 359 lined scientific goals are achievable by deploying gravity missions in orbit.

360 The requirements towards MaQuIs to fulfill the outlined scientific goals are discussed in this paper.  
 361 The following sections will give reasons and context for achievable sensitivities and involved challenges.

## 2.7 Pathfinder

In addition to the mapping of Mars, MaQuIs can serve as a pathfinder mission for future quantum-based gravity field missions. With the technology from MaQuIs, miniaturizing systems and preparing them for reliable operation in deep space, missions to map the gravitational field of different planetary bodies become more and more available. Especially the possibility to measure dynamics of subterranean oceans renders such experiments interesting for future mission to the moons of the gas giants. With appropriate correction of drag, this could also be envisaged to measure the gravitational field of the gas giants themselves.

Other areas of interest, for which MaQuIs could be a pathfinder, are comparative planetology and the study of climate change on other planets and on Earth. For the latter, systems are currently developed, which share a lot of synergy with MaQuIs.

As the name suggests, MaQuIs will make use of quantum technologies to achieve the planned accuracy. In this case, especially cold atom sensors are foreseen in combination with optomechanical inertial sensors and stabilized laser links. With those technologies in place, MaQuIs can act both as a pathfinder for future quantum technologies deployed in space and as a technology driver to develop the necessary setups. The recently developed cold atom roadmap (Alonso et al., 2022) and the summary of quantum physics in space (Belenchia et al., 2022) detail current and planned activities in the area of quantum technologies in space.

## 2.8 Summary of the Scientific Goals

The scientific goals of the mission can be summarized as follows. MaQuIs shall:

- Improve the gravitational field map of Mars
- Detect subsurface structures, especially water occurrences and buried impact craters
- Improve the knowledge of the internal structure of the planet, both crustal and mantle structures
- Determine if current mantle convective processes can be observed
- Monitor seasonal changes on the surface
- Aid in understanding the climate collapse and its comparison to dynamics on Earth
- Measure planetary dynamics and subsurface changes
- Identify areas of increased and decreased density

- 390 • Inform future landing sites
- 391 • Act as a pathfinder for future quantum-based missions, especially to other celestial bodies

### 392 **3 Detection Requirements**

#### 393 **3.1 Expected Signals**

394 The static gravity field (gravity anomaly: gravity minus gravity of reference ellipsoid) of Mars ranges  
 395 from  $-695$  mGal to  $3135$  mGal (Konopliv et al., 2016). The majority of the gravity anomalies do not ex-  
 396 ceed  $\pm 500$  mGal and only the major volcanic regions result in higher gravity anomalies (see also Fig. 1).  
 397 The order of magnitude, excluding these volcanic areas, is comparable to the Earth’s gravity field of about  
 398  $-300$  mGal to  $470$  mGal (Zingerle et al., 2020).

399 The temporal gravity field variations seem to be dominated by  $\text{CO}_2$  exchange between the north-  
 400 ern and southern hemisphere and the tidal potential from the Martian moons, Phobos and Deimos. For  
 401 the mass changes at the poles between Summer and Winter given in section 2.3 the gravity signal at an  
 402 orbit height of  $150$  km to  $200$  km is in the order of  $230$   $\mu\text{Gal}$  using a disc shaped mass distribution and  
 403 a spherical approximation of Mars.

#### 404 **3.2 Noise Sources**

405 For the mission under consideration, the atmospheric drag will be the main disturbing force. It de-  
 406 pends strongly on the spacecraft geometry, the velocity of the spacecraft and the atmospheric density,  
 407 which increases with decreasing orbital altitude. It is difficult to numerically assess it with a high pre-  
 408 cision. General Circulation Models (GCMs) and ionosphere-thermosphere models are commonly used to  
 409 model the atmosphere on large scales, as for example the longitudinal dependence of the atmospheric den-  
 410 sity and its annual changes. But they fail to capture the short term variations in the Martian upper at-  
 411 mosphere, as has been confirmed during operational aerobreaking maneuvers by many previous space mis-  
 412 sions from ESA and NASA (e. g. Castellini et al., 2018).

413 Typically, mismodelling of atmospheric density is accounted for in the determination of planetary  
 414 gravity fields from Doppler data by the estimation of correction terms, such as drag scale factors and em-  
 415 pirical accelerations (Genova et al., 2016). For spacecraft equipped with high-accuracy accelerometers,  
 416 such as the ESA missions BepiColombo to Mercury and the Jupiter Icy Moons Explorer (JUICE), these

417 effects can be directly measured, significantly reducing the potential noise on the gravity field solution  
418 induced by these effects (Cappuccio et al., 2020).

419 Recently, accelerometers on board the Mars Atmosphere and Volatile Evolution (MAVEN) space-  
420 craft have monitored the neutral density in Mars thermosphere (above approximately 120 km). This re-  
421 gion affected by radiation and energy deposition from the Sun and by energy and momentum from the  
422 lower atmosphere orbit-to-orbit variability is found to be still significant (Zurek et al., 2017).

423 For a lower flying mission like MaQuIs atmospheric drag will be significant it is the case for the MAVEN.  
424 Onboard precise accelerometers and inertial measurement units (IMU), similar to those onboard MAVEN,  
425 can measure directly the net acceleration, determine its effect on the orbit and correct for. In addition,  
426 these measurements allow for a better determination of Martian atmospheric properties, which will im-  
427 prove the tracking data analysis of other missions. Atmospheric density measurements along the orbiter  
428 path would yield hydrostatic density and temperature profiles, along track and altitudinal density waves,  
429 and latitudinal and longitudinal density variations (Zurek et al., 2017). Moreover, the surface loading vari-  
430 ability due to atmospheric mass transport will have a measurable influence on the Martian gravity field,  
431 making knowledge of the Martian atmospheric dynamics directly relevant for interpreting measured tem-  
432 poral gravity change.

433 In addition to non-gravitational noise sources the gravitational effects of Phobos and Deimos with  
434 semimajor axes of the respective orbits of 9376 km and 23 463 km have to be taken into account having  
435 a major influence on a spacecraft. For a mission like Mars Global Surveyor, with an orbital height around  
436 400 km, the gravitational effect is larger than atmospheric drag (Konopliv et al., 2006). The masses and  
437 orbits of Phobos and Deimos are therefore estimated in the gravity field recovery process. Unlike atmo-  
438 spheric density, the dynamics of the Martian moons is well constrained and its evolution is predictable  
439 (Lainey et al., 2021), and with proper model consideration, this influence will not pollute the gravity re-  
440 covery.

441 The determination of the Martian gravity field is typically done concurrently with the determina-  
442 tion of its rotational parameters. The relationship between rotation (i.e mainly Length-of-Day but also  
443 Polar motion) and time-variable low degree gravity coefficients has been well established ((Karatekin, Van  
444 Hoolst, Tastet, et al., 2006; Karatekin et al., 2011)). Their determination from single orbiter tracking can  
445 be challenging, partly due to the sensitivity of zonal harmonics to orbiter geometry but also because of  
446 the low-degree zonals obtained from a single orbiter tracking analysis are contaminated by higher-degree

447 harmonics with non-negligible seasonal variations . For the proposed mission, insufficiently accurate de-  
448 termination of the Mars Orientation Parameters (MOPs) could lead to unmodelled rotational variations  
449 being interpreted as temporal gravity field variations at the same frequency. For terrestrial and lunar grav-  
450 ity field determination, this is mitigated by geodetic techniques and LLR, respectively. For Mars, the use  
451 of lander tracking data (such as InSight) will be important (Kuchynka et al., 2014; Folkner et al., 2018),  
452 since these data are sensitive only to rotational variations and not temporal gravity changes.

### 453 **3.3 Link Pointing Requirements**

454 The Laser Ranging Interferometer (LRI) on-board GRACE-FO requires a pointing accuracy of the  
455 laser beams with respect to each other of less than 100  $\mu$ rad (Abich et al., 2019). This requirement is driven  
456 by the amount of received laser power and by the required level of angular overlap of the beams in or-  
457 der to produce a detectable interferometric beat note signal. This has two consequences: 1) A beam steer-  
458 ing mechanism is required to maintain proper beam pointing between the satellites. This is necessary due  
459 to larger orbital variations than 100  $\mu$ rad and performance limits of state-of-the-art spacecraft attitude  
460 and orbit control systems. The mechanism developed for GRACE-FO has demonstrated a pointing er-  
461 ror below 10  $\mu$ rad on ground (Schütze et al., 2014). 2) A link acquisition procedure, potentially includ-  
462 ing the use of dedicated hardware (see Sec. 4.5.1), needs to be foreseen that ensures the sufficient point-  
463 ing of the laser beams on the two spacecraft prior to the instrument’s transition into science mode (Koch  
464 et al., 2018; Koch, 2020).

## 465 **4 Proposed Mission Scenario**

### 466 **4.1 Mission Summary**

467 MaQuIs is proposed as a gravity field mission. It follows the configuration of GRAIL (Zuber et al.,  
468 2013), GRACE (Tapley et al., 2004) and GRACE-FO (Abich et al., 2019) and consequently consists of  
469 two satellites trailing each other, as shown in Figures 3 and 5. The two satellites are connected by an op-  
470 tical link.

471 If one is subjected to an increased gravitational field, e. g. caused by a denser material on or below  
472 the Martian surface, it is accelerated. The acceleration then leads to a variation of the distance between  
473 the two satellites which can be translated into a gravitational signal. This process is sketched in figure 4.

474 The accuracy of the ensuing measurement depends on the stability of the optical link, the correc-  
 475 tion for drag and other non-gravitational accelerations acting on the satellites, the orbital velocity, and  
 476 the distance to the target body.

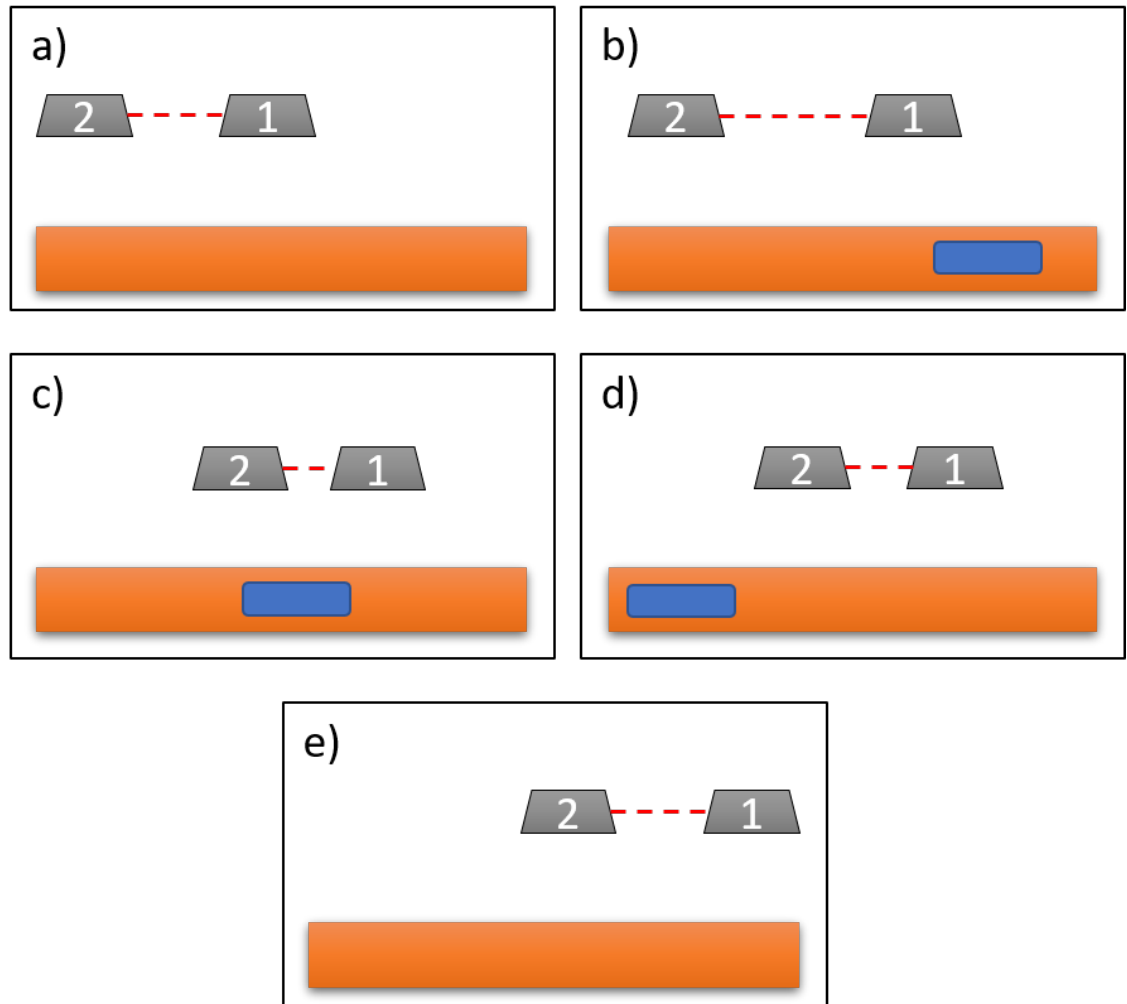


Fig. 4: A sketch to show the measurement principle: Two satellites chasing one-another to measure changes in the gravitational field due to the change in the distance between the satellites. In this sketch it is shown how satellite 2 chases satellite 1 (tabloid a)). If the underground is denser, here represented by the blue rectangle, the first satellite is accelerated by the resulting increased gravitational force (tabloid b)). Once satellite 1 passes that dense portion, it is decelerated, while satellite 2 feels the attractive force. The distance between the two satellites is reduced (c)). With the deceleration of satellite 2 passing (d)), the original distance is re-established (e)). From the variation in distance, the gravitational field is determined.

477

## 4.2 Terrestrial and Lunar Experiments

478

479

480

481

Global gravity missions, mapping the field distribution have been deployed to observe and investigate Earth (Rummel et al., 2011; Tapley et al., 2004). These missions were determined to study, among other goals, the effects of climate change by monitoring sea level rise and oceanic dynamics through gravity field observation (Tapley et al., 2019).



Fig. 5: Artist's impression of the two GRACE-FO spacecraft in orbit around the Earth (credit DLR-SI)

482

483

484

The results of these missions combined with images of the Earth allow for determination of density distribution on Earth and foster understanding of our planet and its inner structure (Mandea et al., 2020).

485

486

487

Additionally, future missions to map the gravity field of the Earth are investigated (Haagmans et al., 2020) to meet the end user demands of gravity field products (Pail et al., 2015). The next generation of gravity measurements from orbit is set to include quantum sensors as inertial measurement units.

488 Several such missions have been proposed. The next steps in quantum sensor development for setups based  
489 on cold atoms is, for instance, outlined by Alonso et al. (2022).

490 Similarly, GRAIL (Zuber et al., 2013), was deployed to understand the inner structure and density  
491 distribution of the Moon (Goossens et al., 2020). While GRAIL did not deploy quantum sensors in its  
492 design, it successfully demonstrated that a gravimeter mission is the desired tool to investigate celestial  
493 bodies in greater detail and higher precision.

### 494 **4.3 Flight Configuration & Orbital Considerations**

495 MaQuIS will be composed of two satellites trailing each other at a distance of at least 200 km. The  
496 distance will be monitored by a bi-directional optical link between the satellites. Star tracker and com-  
497 munication to Earth will ensure tracking of the orbital parameter and thruster on board both satellites  
498 will enable corrections.

499 MaQuIS will be in an areocentric orbit altering the relative inclination due to the rotation of the  
500 planet, scanning the entire planet over time. If, however, it becomes apparent, that a specific region or  
501 that the dynamics of a specific region, such as the polar ice caps during sublimation of the CO<sub>2</sub>, are of  
502 increased interest, this plan could be changed in favour of an uni-planar orbit.

503 The achievable accuracy of the measurement is determined by several factors, two of which are linked  
504 to orbital considerations:

#### 505 1. Orbital Height

506 The orbital height impacts the measurement directly, as the closer to the surface the two satellites  
507 fly, the more pronounced is the effect of the gravity field variations, which can be observed by the  
508 instruments on board the spacecrafts. For comparison, GRAIL orbited the Moon in a lowest al-  
509 titude of 30 km, while GRACE orbited Earth in an altitude of  $\approx 450$  km.

#### 510 2. Atmospheric Density

511 In general, the atmospheric density, and thereby the drag is lower the further an orbiting satellite  
512 is dispatched from the planet. With increasing atmospheric density, two effects have to be consid-  
513 ered:

- 514 • vibrational noise due to residual accelerations and
- 515 • limitations on the mission life time due to deceleration of the satellites.

516 In order to achieve the targeted sensitivity a trade-off has to be made between the orbital height and the  
517 acceptable atmospheric drag. On ground level Mars' atmospheric density is only 6 hPa, about 0.6 % of  
518 Earth's atmospheric density. However, the density does not decrease with altitude as rapidly as is the  
519 case for Earth. Hence, an orbit higher than that of GRAIL above the Moon but lower than that of GRACE  
520 above the Earth can be chosen for MaQuIs with respect to Mars. Flying at a lower altitude allows for  
521 a better determination of the gravity field, both in terms of degree strength and uncertainty. However,  
522 the influence of atmospheric drag increases with lower altitude, which requires a more propellant and/or  
523 a different orbit control system (such as continuous low thrust) to maintain the orbit for a sufficient amount  
524 of time. At an altitude of 170 km, the mean atmospheric density is roughly similar to that experienced  
525 by the GOCE spacecraft at Earth, on the order of  $10^{-11}$  kg/m<sup>3</sup>. At 200 km and 250 km, it is on aver-  
526 age one and two orders of magnitude smaller, respectively, while at 100 km it is three orders of magni-  
527 tude larger than for GOCE. This trade off will depend on the ballistic coefficient of the satellites, the  
528 mass and power budget available for the propulsion system, requirements on static and temporal grav-  
529 ity field determination quality, variability of the Martian atmospheric density, risk trade-offs, etc. A com-  
530 prehensive system study should be performed to trade off these various aspects.

531 Other contributing noise factors, also those stemming from orbital choices, are summarized in the  
532 following chapters as well as the targeted sensitivity.

#### 533 **4.4 Target Sensitivity**

534 As it is discussed above, the subsurface lakes are in the order of 10 km in diameter. The surface ice  
535 sheets have been measured to be in the order of several hundreds to thousand kilometers in diameter with  
536 thickness in the order of several kilometer.

537 While other scientific goals have been determined, the detection of the subsurface water reservoirs  
538 is the central scientific goal. It simultaneously is the most challenging. The detection of the subsurface  
539 water reservoirs does not only depend on their diameter, but mainly on their volume. To resolve the cur-  
540 rently discussed occurrences, a spatial resolution for static measurements on ground in the order of sev-  
541 eral tens of kilometers is targeted by MaQuIs. In case of static measurements, averaging over several mea-  
542 surements and orbits, and thereby periods of time, is possible and increases sensitivity. The resolution  
543 for dynamical processes can be relaxed, since those target primarily the sublimation and deposition of  
544 large amounts of CO<sub>2</sub> on the poles.

## 4.5 Payload Design

### 4.5.1 Primary Instrument

As was the case for both the GRACE and GRACE-FO missions, the two satellites are equipped with the same systems. Figure 6 outlines the primary instrument design, without any redundancy measures. The figure schematically illustrates the combination of a laser interferometer ((a)-(e)) and a hybrid quantum sensor ((g) and (f)). Thereby, the laser interferometer is sketched as an off-axis design, building on the layout of the successful LRI. At a later stage it will have to be evaluated whether an off-axis or an on-axis design (where the received and transmitted laser beams share a common optical path) is advantageous in the context of the overall mission. For this, the required level of redundancy, the inter-satellite distance and other parameters will have to be taken into account. The optical link is received at entry point (c) from which it travels to the optical bench at (d). There the interference signal between the received beam and the locally generated beam (e) is obtained. The link then proceeds to the beam routing optics at (a), which are surveyed by a combination of the optomechanical inertial measurement unit (f) and the atom interferometer (g). Eventually, the light is transmitted to the other spacecraft via the exit pupil at (b). The other satellite includes the same setup and is mirrored with respect to the first satellite. In the following, the systems are explained individually.

The sketch also shows the acceleration of the satellite  $\vec{a}$  along the shown axis. Accelerations along other axes, as well as rotation, have to be treated equivalently.

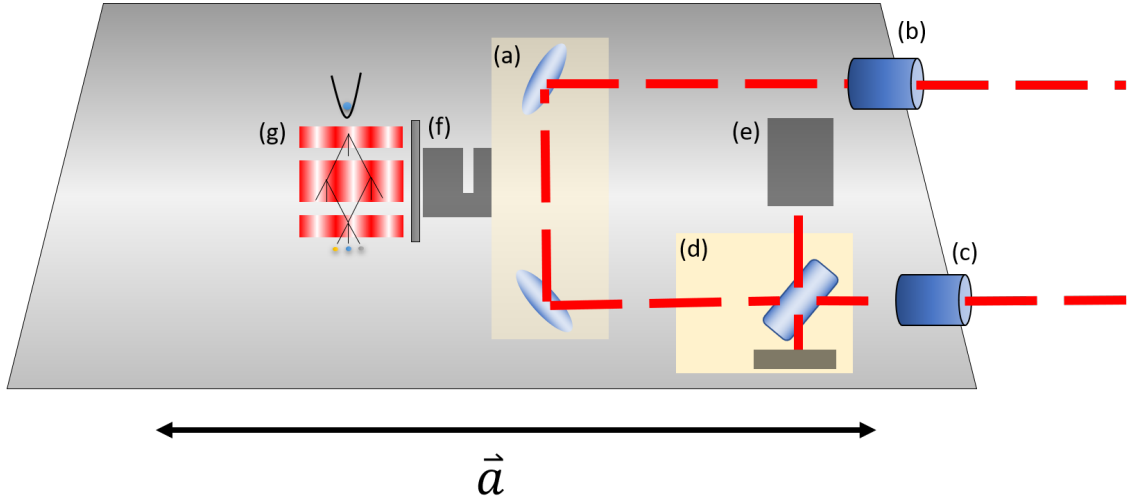


Fig. 6: This sketch outlines the primary instrument. It consists of the laser link between the two satellites, which comes in at point (c), is then combined with the signal of the stabilized internal laser (e) on an optical bench (d), where the beat between the two signals is measured. The laser beam is then guided towards the exit aperture (b) via the beam routing optics at (a), which are situated as close to the center of mass of the spacecraft as possible to reduce residual accelerations. The beam routing optics are surveyed by a combination of quantum accelerometers (optomechanical inertial measurement unit, OMIS (f) and the cold atom interferometer (g)). Finally, the laser signal is sent to the other satellite through (b), where the system is mirrored.

The vector  $\vec{a}$  shows the acceleration of the satellite due to, for instance, atmospheric noise.

The sketch shows one dimension, the other dimensions have to be treated separately.

The following paragraphs describe the components that make up the primary instrument:

**Laser Ranging:** Both spacecrafts share an interferometric bidirectional laser link to measure relative changes in the distance between the two satellites. This distance measurement depends on the chosen laser wavelength. For this mission, a wavelength in the infrared (1064 nm to 1550 nm) is envisioned due to flight heritage and the availability of well-suited components, e. g. optics, lasers and resonators. As stated previously, both spacecrafts host identical hardware. For the purpose of laser ranging this includes: lasers (Bachman et al., 2017), optical benches (Abich et al., 2019; Dahl et al., 2016), potentially retroreflectors (Dahl et al., 2016), instrument control (Bachman et al., 2017) and laser frequency reference units (Thompson et al., 2011; Sanjuan et al., 2019).

572 Space proven interferometric link technologies and laser modules exist and have been developed for  
573 several different applications, including deep space missions such as LISA (Antonucci et al., 2012). The  
574 Laser Ranging Interferometer of the satellite gravimetry mission GRACE-FO, successfully operating since  
575 2018, reaches a noise level of about  $10 \text{ nm}/\sqrt{\text{Hz}}$  at 40 mHz and about  $300 \text{ pm}/\sqrt{\text{Hz}}$  at 1 Hz (Abich et al.,  
576 2019). For frequencies below 30 mHz gravity dominates the ranging signal and it is not possible to di-  
577 rectly evaluate the interferometer noise floor. However, thorough modelling of the LRI and comparison  
578 with GRACE-FO microwave ranging data suggests that the well-understood tilt-to-length coupling ef-  
579 fect, which can be subtracted in post-processing, and laser frequency noise remain the LRI's limiting noise  
580 sources in the  $\mu\text{Hz} - \text{mHz}$  frequency range (Müller et al., 2022).

581 As laser frequency noise is the dominant noise source for a laser interferometer with such unequal  
582 arm lengths as is proposed here, the laser frequency must be actively stabilized. Thereby, two distinct  
583 timescales are of importance: short timescales between 10 s to 1000 s, on which the local gravity field un-  
584 derneath the spacecraft is sampled, and timescales of months and years which are important for the track-  
585 ing of long-term changes of the local gravity field. For the stability requirement on the shorter timescales  
586 an optical cavity with optional thermal shielding appears to be the prime candidate (Sanjuan et al., 2019).  
587 The longer timescales requirement could be met by minimally invasive measures to the experimental setup  
588 to further enhance the stability of these optical cavities. Applicable techniques are currently under in-  
589 vestigation in the context of the next generation of Earth gravity field missions (Rees et al., 2021, 2022).

590 One of the most critical steps in the commissioning phase of an intersatellite laser interferometer  
591 is the initial establishment of the laser link (Koch et al., 2018). In order for the interferometer to func-  
592 tion properly the laser beams that are transmitted by both spacecraft have to be aligned to each other  
593 with a maximum error on the order of about  $\pm 100 \mu\text{rad}$ . Additionally, the frequencies of the involved lasers  
594 must match to within the photoreceiver bandwidth of  $\leq 37 \text{ MHz}$  (Fernández Barranco et al., 2018). Ground-  
595 to-orbit effects, bias angles between interferometer sub-units and other systems on the platform (e.g. star  
596 trackers) caused by mechanical tolerances during integration of the units as well as thermally-induced  
597 deformations of the spacecraft are the main drivers for a knowledge error regarding the true line of sight  
598 between two spacecraft. Hence, an alignment of the laser beams by means of dead reckoning will most  
599 probably not be successful. In the absence of absolute laser frequency references also the laser frequency  
600 difference of the involved lasers would not match to within the required level due to temperature differ-  
601 ences of the different spacecraft and corresponding effects on the lasers and cavities. An appropriate pro-  
602 cedure to calibrate this 5-dimensional uncertainty space (two angles per spacecraft and the laser differ-

603 ence frequency) should foresee a dedicated link acquisition system (LAS) on each spacecraft (Koch, 2020).  
 604 These may include dedicated acquisition light sources that are specifically tuned to the needs of this crit-  
 605 ical mission phase and sensors that are designed to perform an incoherent detection of any incoming sig-  
 606 nal. A LAS thus drastically reduces the complexity of the associated link acquisition procedure and can  
 607 provide a major positive impact to the risk reduction scheme. Especially for a remote mission which or-  
 608 bits another celestial body the latter point is quite significant.

609 While the components briefly described above define a baseline laser interferometer configuration,  
 610 different technology options should be considered:

611 In addition to the stability of the laser frequency, which can be realized by using optical cavities,  
 612 its absolute value is also of interest as the ranging measurement directly scales with it. Hence, an addi-  
 613 tional absolute frequency reference, e. g. an iodine cell, could be incorporated (Döringshoff et al., 2017).

614 In the absence of sophisticated GNSS navigation, a measurement of the intersatellite distance by  
 615 using the interferometric laser link seems beneficial. In the context of the LISA mission this technique  
 616 was developed and tested on ground (Sutton et al., 2010; Heinzel et al., 2011). With only minor addi-  
 617 tional hardware absolute distance measurements between two spacecrafts below 0.4 m were achieved with  
 618 an update rate on the order of a few Hertz (Sutton et al., 2010; Heinzel et al., 2011).

619 Using the same additional hardware, rudimentary communication protocols can be implemented  
 620 using the interferometric laser link. On-ground experiments showed the functionality with data rates of  
 621 up to 20 kbps (Sutton et al., 2010; Heinzel et al., 2011). This technique seems especially compelling as  
 622 it can be used to transfer data between the spacecraft and only have one of the satellites communicate  
 623 with Earth. This measure saves energy and underscores the inherent redundancy scheme that is realized  
 624 by implementing two identical spacecraft.

625 **Inertial Measurement Unit:** Non-gravitational acceleration, e.g. due to atmospheric drag or ra-  
 626 diative pressure, can obscure the results obtained by the laser link (Kornfeld et al., 2019; Tapley et al.,  
 627 2004). Additional accelerometers onboard of the satellites enable the reduction of spurious accelerations  
 628 (Kornfeld et al., 2019; Christophe et al., 2015; Tapley et al., 2004). Current approaches rely on electro-  
 629 static accelerometers, that suffer from drifts at low frequencies (Zahzam et al., 2022; Klinger & Mayer-  
 630 Gürr, 2016; Carraz et al., 2014; Touboul et al., 2012). In this context, atom interferometers (AI) were  
 631 proposed to replace (Lévêque et al., 2021; Migliaccio et al., 2019; Trimeche et al., 2019; Chiow et al., 2015)  
 632 or complement the classical accelerometers (Zahzam et al., 2022). By principle, atom interferometers can  
 633 provide absolute and long-term stable measurements with noise levels of  $42 \text{ nm s}^{-2} \text{ Hz}^{-1/2}$  and  $0.5 \text{ nm s}^{-2}$

634 after averaging, as demonstrated in atom interferometric gravimeters (Ménoret et al., 2018; Freier et al.,  
635 2016; Hu et al., 2013; Louchet-Chauvet et al., 2011; Peters et al., 1999). Operation in a microgravity en-  
636 vironment could boost the sensitivity of such sensors by increasing the free-fall time of the atoms during  
637 the interferometry sequence, a critical parameter for the scaling factor (Kasevich & Chu, 1991), leading  
638 to anticipated noise levels of  $0.1 \text{ nm s}^{-2} \text{ Hz}^{-1/2}$  and below (Dickerson et al., 2013). Multiple experiments  
639 implemented and investigated atom optics and atom interferometry in microgravity, including the pro-  
640 duction of Bose-Einstein condensates followed by a matter-wave collimation step, enabling the ultra-low  
641 expansion rates of the atomic ensembles for compatibility with extended free-fall times (Gaaloul et al.,  
642 2022; Lachmann et al., 2021; Aveline et al., 2020; Becker et al., 2018; Rudolph et al., 2015; Müntinga et  
643 al., 2013; Geiger et al., 2011; van Zoest et al., 2010). Operating atom interferometers at high data rates  
644 currently either implies an increased noise level due to short free-fall times (Rakholia et al., 2014) or an  
645 increased complexity when implementing an interleaved mode (Savoie et al., 2018). An alternative is the  
646 hybridisation with an additional sensor to realise a combined drift-free system with sufficient bandwidth (Zahzam  
647 et al., 2022; Richardson et al., 2020; Lautier et al., 2014). The usage in inertial measurement units re-  
648 quires additional investigation, which is in synergy with current developments for an Earth-orbit grav-  
649 ity mission.

650 The AI system detection bandwidth is limited by the Nyquist sampling criterion to half the mea-  
651 surement repetition rate. In order to increase the bandwidth, a supplemental sensor will be used with  
652 the AI system. Optomechanical inertial sensors (OMIS) combine high precision displacement metrology  
653 with a low-noise mechanical oscillator to detect input acceleration down to the thermal noise limit with  
654 a bandwidth of several kHz or more. These sensors can be directly constructed into the AI retroreflect-  
655 ing mirror to provide excellent overlap of their common reference frames easing correlation analysis be-  
656 tween the two systems. Further, the optical source can be shared between the two systems, if desired,  
657 for reducing payload size. OMIS share a lot of features with optical cavity based frequency references such  
658 as low drift and high measurement precision. Additionally, the calibration parameters are tied to the sta-  
659 bility of the onboard clock source and this is often the most precise and stable device in the system. This  
660 combination of features improves the low-frequency portion of the OMIS bandwidth enough to provide  
661 good overlap with demonstrated AI system bandwidths at a similar level of measurement imprecision.  
662 In this way, the AI can provide drift control of the OMIS while the OMIS provides high speed measure-  
663 ment of the residual accelerations affecting the satellite.

664       **Pointing:** The accuracy of the measurement depends on the knowledge of the orbit (see below) and  
665 the alignment of the satellites to ground. Several techniques exist to establish the necessary precision to  
666 achieve the scientific goals.

667       The alignment of the satellites can be regularly controlled by using the atom interferometer at reg-  
668 ular intervals as a gradiometer. For this purpose, a secondary atom cloud needs to be suspended radi-  
669 ally above the first. If the measured gravity gradient is not in line with predictions, the satellite align-  
670 ment has to be corrected. While this method is certainly intriguing, classical means are foreseen for MaQuIs.

671       **Propulsion:** As part of the attitude and orbital control (AOCS), the amount of necessary propel-  
672 sion as well as the positioning will have to be discussed. MaQuIs will fly in a low orbit and orbital cor-  
673 rections as well as alignment corrections will become necessary. For this purpose additional propulsion  
674 and appropriate thruster will be implemented. This part of the payload is mentioned here as it could prove  
675 an important mass driver.

676       **Spacecraft Positioning:** The orbit of satellites around other planetary bodies are usually deter-  
677 mined by radio Doppler measurements from the Earth. The X-band Doppler radio accuracy for the Mars  
678 Reconnaissance Orbiter (MRO) is in the order of 0.05 mm/s (Genova et al., 2016) depending on Sun-Earth-  
679 Mars angle. The requirement ( $3\sigma$ ) for the MRO spacecrafts relative position to Mars is 100 m in the along  
680 track, 40 m cross track and 1.5 m in the radial direction. Results from the mission show and RMS of 3.9 m,  
681 0.6 m and 0.9 m respectively (Highsmith et al., 2008). For MaQuIs, where unlike tracking-based gravity  
682 field solutions the position uncertainty does not translate directly into gravity field uncertainty (provided  
683 the orbit is sufficiently accurate), it is expected that a typical two-way coherent X-band Doppler link will  
684 be sufficient, and accuracy enhancements from for instance X/Ka-band tracking as is done for BepiColombo  
685 (Iess et al., 2021) will not be necessary. Possible complementary range and VLBI data will not help to  
686 improve the spacecraft orbits w.r.t Mars, but would be beneficial for continued improvement of the Mar-  
687 tian ephemeris (Dirkx et al., 2017, 2019), and possible orbit validation.

688       The orbit determination also depends on variation of center of mass (COM) with respect to the ra-  
689 dio antenna phase center (Cascioli & Genova, 2021), which can be in the decimeter range (Genova et al.,  
690 2016) e. g. due to orientation changes of the radio antenna to ensure its pointing towards the Earth or  
691 rotations of the solar panels to align with the Sun. For spacecraft like the MRO with a movable high gain  
692 antenna and solar panels (see Fig 7), a mechanical model is required to calculate the COM depending  
693 on the mass distribution of the satellite components and its fuel consumption (Cascioli & Genova, 2021).

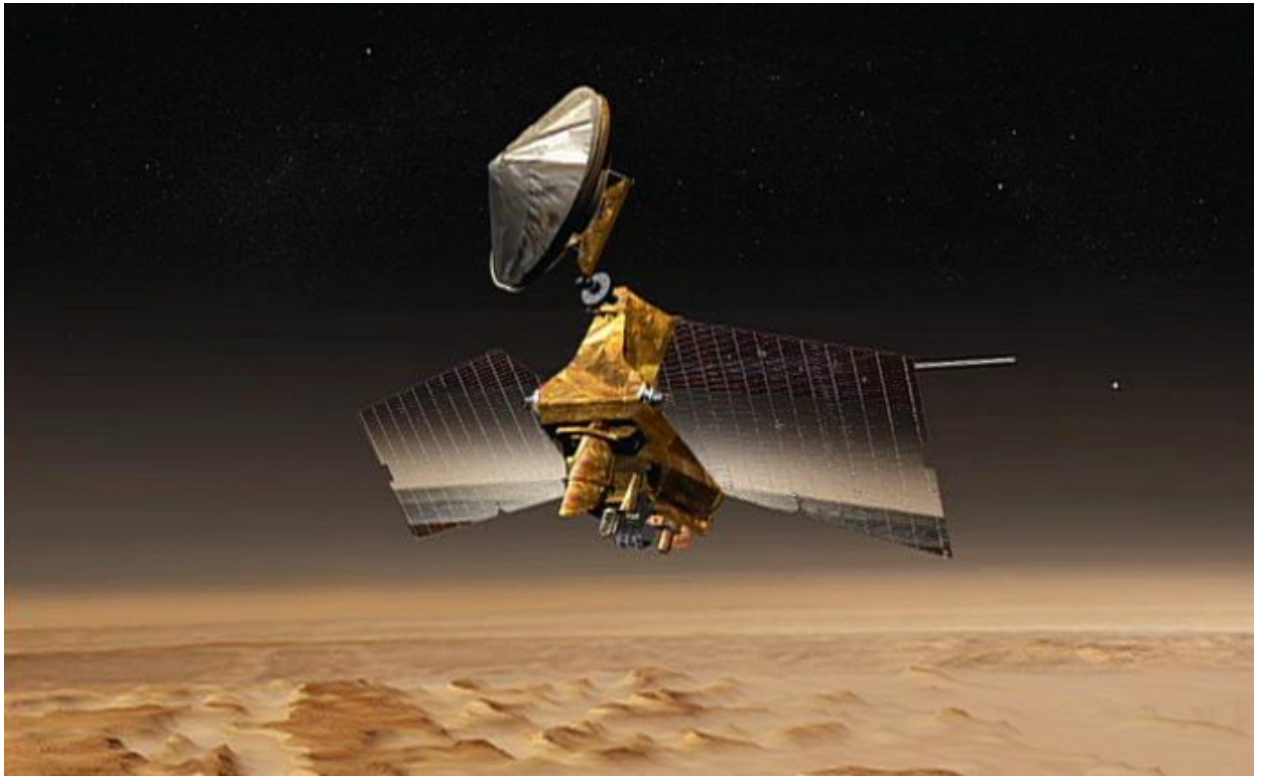


Fig. 7: Mars Reconnaissance Orbiter (artist rendering, credit NASA/JPL-Caltech) with a 3 m High Gain Antenna and 10 m<sup>2</sup> solar panels.

694 On a number of recent missions, such as BepiColombo and JUICE, an accelerometer is used to mea-  
695 sure non-conservative forces, including variations of the change in spacecraft center of mass due to for  
696 instance effects of propellant sloshing (Cascioli & Genova, 2021; Iess et al., 2021).

697 These aspects have not been an issue with terrestrial satellite gravimetry missions, because offsets  
698 between star cameras, GNSS antennas and the CMO are relatively static during one orbit due to fixed  
699 solar panels and antennas (see Fig. 5). However, for MaQuIs the aforementioned considerations might  
700 become relevant. The requirement for the GRACE-FO mission for the short term stability (one orbit)  
701 of the COM with respect to the accelerometer testmass is  $\pm 9 \mu\text{m}$ . Long term variations (six months) of  
702 COM movements, e. g. due to fuel consumption, are kept within  $\pm 100 \mu\text{m}$  by employing movable mass  
703 trim mechanisms (Kornfeld et al., 2019). The evaluation of GRACE-FO LRI data has shown the abil-  
704 ity of the attitude and orbit control system (AOCS) to maintain the pitch and yaw variations of the satel-

705 lite pair within  $\pm 100 \mu\text{rad}$  (Goswami et al., 2021), which is the technical requirement of the LRI. Addi-  
706 tionally, the combination of differential wavefront sensing and the beam steering mechanism with the star  
707 camera and IMU show the potential for an improved accuracy for attitude determination.

708 **Mission Lifetime:** One of the limitations of the mission is its lifetime. To measure the gravita-  
709 tional field distribution, an orbit, as close as possible to the surface is preferential. In the case of GRAIL,  
710 for instance, a low orbit over the lunar surface, with only 30 km height was chosen (Zuber et al., 2013).  
711 This was possible due to the lack of atmosphere on the moon. In case of GRACE, GRACE-FO, and GOCE  
712 higher altitudes had to be chosen to allow for the required mission lifetimes within Earth's atmosphere.

713 Similar considerations have to be taken into account for MaQuIs. The final orbital considerations  
714 will be a trade-off between atmospheric drag, available fuel, acceptable vibrations, and required mission  
715 lifetime.

716 At this time a mission lifetime of at least two Martian years is planned. This allows for the study  
717 of annual processes and enable comparability between two sets of measurements in a given annual po-  
718 sition. This choice has implications on a reasonable orbital altitude, satellite design, as well as fuel-consumption.

#### 719 *4.5.2 Additional Instruments*

720 **Mass Spectrometer:** The primary Instrument is the laser ranging facility including the support-  
721 ing technology. In addition, knowledge of the atmospheric density and composition at the orbit is im-  
722 portant. It is therefore conceivable to include a mass spectrometer in the payload.

723 The atmospheric disturbances could also be measured using the atom interferometer without the  
724 additional mass spectrometer. The drag on the satellites yields information on atmospheric density and  
725 phenomena such as gravity waves (Starichenko et al., 2021) within those. Consequently, measuring the  
726 forces acting on the satellite allows scientific studies of the Martian atmosphere and its dynamics in ad-  
727 dition to the gravitational field mapping.

728 **Imaging Technology:** As it is mentioned above, the gravitational data should be supplemented  
729 with imaging data. The correlation between images and the recorded gravitational data yields the infor-  
730 mation on the ground below. Of course, several high-resolution images of Mars exist. To supplement the  
731 gravitational data and account for any temporal changes, an additional camera on MaQuIs is beneficial.  
732 As, in addition, available cameras are not taking up a high portion of the available size, mass, and power  
733 budget. Consequently, flying a camera on MaQuIs will allow to correlate the gravity data directly to im-

734 ages taken during flight. Space qualified cameras are readily available and should be implemented into  
735 the payload.

### 736 **4.5.3 Technology Readiness Level**

737 Currently, the items in the payload are advanced with respect to the technology readiness level (TRL)  
738 and promise reliable operation and precise measurements. The least evolved system is the atom inter-  
739 ferometer, allowing for the drift-free correction of the inertial measurement unit. As it is described above,  
740 condensed atom ensembles have already been deployed in space. The adaptations necessary to deploy such  
741 a system in space are supported and with similar missions planned for Earth, the technology will be read-  
742 ily available at the time of proposed launch for MaQuIs.

743 For most of the other components, commercial, space qualified items are available or other hard-  
744 ware with space heritage exists. While MaQuIs will opt for non-qualified items, for all items a qualified  
745 option exists, that could be exchanged if the technology proves too immature. This is especially true, since  
746 the system will fly in a GRACE-configuration and could therefore rely on the developments for GRACE,  
747 GRACE-FO, and GRAIL.

748 Additional developments of the required technologies are outlined in the cold atoms roadmap (Alonso  
749 et al., 2022). This shows the increased interest in cold atom technology for scientific and applied missions  
750 and the required developments to establish the necessary systems for different missions. MaQuIs both,  
751 benefits from and drives these developments.

## 752 **4.6 Noise Sources**

753 The missions success relies on understanding noise sources and mitigating their impact. The dis-  
754 cussed noise sources in this proposal are:

- 755 • Residual accelerations of the satellites leads to an incorrect measurement. To correct for this, two  
756 inertial measurement units are proposed for MaQuIs. An additional means of reducing the impact  
757 of atmospheric drag is the satellite design, similar to the GOCE mission (Rummel et al., 2011)
- 758 • Undetected orbital variations will lead to a difference in the measured signal and thereby in a faulty  
759 analysis of the data in post processing. Orbital surveillance and correction are therefore paramount  
760 for the success of the mission.

- The laser wavelength deployed for the link between the two satellites determines the accuracy of the measurement. Hence, knowledge about its absolute value in orbit is required.
- Due to the unequal arm lengths of the laser interferometer that shall be used for the inter-satellite distance measurements, laser frequency noise dominates the range measurement. (Bachman et al., 2017; Müller et al., 2022) MaQuIs will deploy optical frequency references to increase the laser stability.
- Thermal fluctuations impact several systems of the satellites resulting in an elevated noise floor.
- Cosmic radiation and light pollution can lead to damage in the system or faulty measurements.

## 5 Additional Gradiometer

On Earth, the only satellite gradiometry mission flown to date was GOCE (Rummel et al., 2011), which determined the global static gravity field with unprecedented accuracy. The noise of the gradiometer axes was approximately  $10 \text{ mE}/\sqrt{\text{Hz}}$ . Further improvements or resolving temporal variations of the gravity field would require major improvements in the satellite design and a reduction of the measurement noise to  $5 \text{ mE}/\sqrt{\text{Hz}}$  or below. In parallel to studies investigating cold atom interferometry on GRACE-FO type missions, in which the cold atom interferometer acts as an accelerometer, gradiometry mission designs based on quantum technologies are also the topic of numerous studies. A quantum gradiometer employs two spatially separated clouds of (ultra-)cold atoms which interact with the same laser beams. This requires a vacuum chamber of a size to accommodate the desired separation, e. g. 50 cm for each axis.

The works by, for example, Douch et al. (2018), Trimeche et al. (2019) and Migliaccio et al. (2019, 2022) discuss different scenarios for employing GOCE type mission scenarios utilising a cold atom interferometer based single axis gradiometer. The proposed instrument and mission designs show a clear benefit in determining temporal gravity field variations as well as geophysical processes when compared to GOCE and in some scenarios even GRACE. However, the main technical challenges, in addition to realising a gradiometer in space, arise from the rotation of the satellite about its along track axis (Lan et al., 2012). A full 3-axis gradiometer could solve this challenge while increasing the complexity of the instrument. A discussion on the rotation of an along track quantum accelerometer can be found, e. g., in (Meister et al., 2022). A compromise in the gradiometer design would be a single axis gradiometer in the cross track direction, greatly reducing rotational effects but not sufficient on its own to exceed GOCE performance levels (Douch et al., 2018), employed on GRACE like mission (Rosen, 2021). This design

790 adds observations perpendicular to the LRI measurements thereby effectively reducing the aliasing er-  
 791 rors in GRACE solutions commonly referred to as striping effect.

## 792 **6 Summary and Outlook**

793 The Mars Quantum Gravity Mission (MaQuIs) targets Mars and its gravitational field to investi-  
 794 gate the planet for subsurface water occurrences. With this capability, MaQuIs is qualified to contribute  
 795 to the discussion around the occurrence of liquid or frozen subsurface water on Mars. Furthermore, the  
 796 study of the gravitational field yields information on planetary dynamics and seasonal changes, interest-  
 797 ing for planetary research.

798 Within this paper we discussed the currently available technologies to execute a complex gravita-  
 799 tional field measurement to improve the available gravitational maps using quantum technologies.

## 800 **7 Data Availability Statement**

801 The paper proposes a mission scheme which does not include any underlying data or software for  
 802 analysis. In consequence there is no data that we can make available or which needs to be published or  
 803 made publicly available.

## 804 **References**

- 805 Abich, K., Abramovici, A., Amparan, B., Baatzsch, A., Okiihiro, B. B., Barr, D. C., . . . others  
 806 (2019). In-orbit performance of the GRACE follow-on laser ranging interferometer. *Physi-  
 807 cal Review Letters*, *123*(3), 031101. doi: 10.1103/PhysRevLett.123.031101
- 808 Alonso, I., Alpigiani, C., Altschul, B., Araújo, H., Arduini, G., Arlt, J., . . . Zupanič, E. (2022). Cold  
 809 atoms in space: community workshop summary and proposed road-map. *EPJ Quantum Tech-  
 810 nology*, *9*(1), 30. doi: 10.1140/epjqt/s40507-022-00147-w
- 811 Antonucci, F., Armano, M., Audley, H., Auger, G., Benedetti, M., Binetruy, P., . . . others  
 812 (2012). The lisa pathfinder mission. *Classical and Quantum Gravity*, *29*(12), 124014. doi:  
 813 10.1088/0264-9381/29/12/124014
- 814 Aveline, D. C., Williams, J. R., Elliott, E. R., Dutenhoffer, C., Kellogg, J. R., Kohel, J. M., . . .  
 815 Thompson, R. J. (2020). Observation of bose-einstein condensates in an earth-orbiting research  
 816 lab. *Nature*, *582*(7811), 193–197. doi: 10.1038/s41586-020-2346-1

- 817 Bachman, B., de Vine, G., Dickson, J., Dubovitsky, S., Liu, J., Klipstein, W., . . . Woodruff, C.  
818 (2017). Flight phasemeter on the laser ranging interferometer on the grace follow-on mission.  
819 *IOP Conf. Series: Journal of Physics: Conf. Series*, *840*, 012011. doi: 10.1088/1742-6596/840/  
820 1/012011
- 821 Banerdt, W. B., Smrekar, S. E., Banfield, D., Giardini, D., Golombek, M., Johnson, C. L., . . . others  
822 (2020). Initial results from the insight mission on mars. *Nature Geoscience*, *13*(3), 183–189.  
823 doi: 10.1038/s41561-020-0544-y
- 824 Becker, D., Lachmann, M. D., Seidel, S. T., Ahlers, H., Dinkelaker, A. N., Grosse, J., . . . Rasel,  
825 E. M. (2018). Space-borne Bose–Einstein condensation for precision interferometry. *Nature*,  
826 *562*, 391–395. doi: 10.1038/s41586-018-0605-1
- 827 Belenchia, A., Carlesso, M., Ömer Bayraktar, Dequal, D., Derkach, I., Gasbarri, G., . . . Bassi, A.  
828 (2022). Quantum physics in space. *Physics Reports*, *951*, 1-70. (Quantum Physics in Space)  
829 doi: 10.1016/j.physrep.2021.11.004
- 830 Belleguic, V., Lognonné, P., & Wiczorek, M. (2005). Constraints on the martian lithosphere from  
831 gravity and topography data. *Journal of Geophysical Research: Planets*, *110*, E11005. doi: 10  
832 .1029/2005JE002437
- 833 Beuthe, M., Le Maistre, S., Rosenblatt, P., Pätzold, M., & Dehant, V. (2012). Density and litho-  
834 spheric thickness of the tharsis province from mex mars and mro gravity data. *Journal of Geo-*  
835 *physical Research: Planets*, *117*, E04002. doi: 10.1029/2011JE003976
- 836 Bibring, J.-P., Langevin, Y., Mustard, J. F., Poulet, F., Arvidson, R., Gendrin, A., . . . Neukum, G.  
837 (2006). Global mineralogical and aqueous mars history derived from omega/mars express data.  
838 *Science*, *312*(5772), 400-404. doi: 10.1126/science.1122659
- 839 Bierson, C. J., Tulaczyk, S., Courville, S. W., & Putzig, N. E. (2021). Strong MARSIS Radar Reflec-  
840 tions From the Base of Martian South Polar Cap May Be Due to Conductive Ice or Minerals.  
841 *Geophysical Research Letters*, *48*(13), e93880. doi: 10.1029/2021GL093880
- 842 Bott, M. H. P. (1960, March). The use of Rapid Digital Computing Methods for Direct Gravity In-  
843 terpretation of Sedimentary Basins. *Geophysical Journal*, *3*(1), 63-67. doi: 10.1111/j.1365-246X  
844 .1960.tb00065.x
- 845 Bouley, S., Baratoux, D., Matsuyama, I., Forget, F., Séjourné, A., Turbet, M., & Costard, F. (2016).  
846 Late tharsis formation and implications for early mars. *Nature*, *531*(7594), 344–347. doi: 10  
847 .1038/nature17171

- 848 Bouman, J., Ebbing, J., & Fuchs, M. (2013). Reference frame transformation of satellite gravity gra-  
849 dients and topographic mass reduction. *Journal of Geophysical Research: Solid Earth*, *118*(2),  
850 759-774. doi: 10.1029/2012JB009747
- 851 Broquet, A., & Andrews-Hanna, J. C. (2022). Geophysical evidence for an active mantle plume un-  
852 derneath elysium planitia on mars. *Nature Astronomy*. doi: 10.1038/s41550-022-01836-3
- 853 Brož, P., Hauber, E., van de Burgt, I., Å pillar, V., & Michael, G. (2019, March). Subsurface Sed-  
854 iment Mobilization in the Southern Chryse Planitia on Mars. *Journal of Geophysical Research*  
855 (*Planets*), *124*(3), 703-720. doi: 10.1029/2018JE005868
- 856 Byrne, S. (2009, May). The Polar Deposits of Mars. *Annual Review of Earth and Planetary Sciences*,  
857 *37*(1), 535-560. doi: 10.1146/annurev.earth.031208.100101
- 858 Cappuccio, P., Di Ruscio, A., Iess, L., & Mariani, M. J. (2020). Bepicolombo gravity and rotation  
859 experiment in a pseudo drag-free system. In *Aiaa scitech 2020 forum*. American Institute of  
860 Aeronautics and Astronautics. doi: 10.2514/6.2020-1095
- 861 Carr, M. H., & Head, J. W. (2015). Martian surface/near-surface water inventory: Sources,  
862 sinks, and changes with time. *Geophysical Research Letters*, *42*(3), 726-732. doi: 10.1002/  
863 2014GL062464
- 864 Carraz, O., Siemes, C., Massotti, L., Haagmans, R., & Silvestrin, P. (2014). A spaceborne gravity  
865 gradiometer concept based on cold atom interferometers for measuring earth's gravity field. *Mi-  
866 crogravity Science and Technology*, *26*(3), 139-145. doi: 10.1007/s12217-014-9385-x
- 867 Carter, J., Riu, L., Poulet, F., Bibring, J.-P., Langevin, Y., & Gondet, B. (2023, January). A Mars  
868 orbital catalog of aqueous alteration signatures (MOCAAS). *Icarus*, *389*, 115164. doi: 10.1016/  
869 j.icarus.2022.115164
- 870 Cascioli, G., & Genova, A. (2021). Precise orbit determination technique to refine spacecraft mechan-  
871 ical modeling. *Journal of Spacecraft and Rockets*, *58*(2), 581-588. doi: 10.2514/1.A34922
- 872 Castellini, F., Bellei, G., & Godard, B. (2018). Flight dynamics operational experience from exomars  
873 tgo aerobraking campaign at mars. In *2018 spaceops conference*. 28.05.-01.06.2018, Marseille,  
874 France. doi: 10.2514/6.2018-2537
- 875 Chiow, S.-W., Williams, J., & Yu, N. (2015). Laser-ranging long-baseline differential atom interfer-  
876 ometers for space. *Phys. Rev. A*, *92*(6), 063613. doi: 10.1103/PhysRevA.92.063613
- 877 Christophe, B., Boulanger, D., Foulon, B., Huynh, P. A., Lebat, V., Liorzou, F., & Perrot, E.  
878 (2015). A new generation of ultra-sensitive electrostatic accelerometers for GRACE Follow-

- 879 on and towards the next generation gravity missions. *Acta Astronaut*, *117*, 1–7. doi:  
880 10.1016/j.actaastro.2015.06.021
- 881 Clifford, S. M., Lasue, J., Heggy, E., Boisson, J., McGovern, P., & Max, M. D. (2010, July). Depth  
882 of the Martian cryosphere: Revised estimates and implications for the existence and detection  
883 of subpermafrost groundwater. *Journal of Geophysical Research (Planets)*, *115*(E7), E07001.  
884 doi: 10.1029/2009JE003462
- 885 Cuřín, V., Broř, P., Hauber, E., & Markonis, Y. (2023, January). Mud flows in southwestern Utopia  
886 Planitia, Mars. *Icarus*, *389*, 115266. doi: 10.1016/j.icarus.2022.115266
- 887 Dahl, C., Baatzsch, A., Dehne, M., Herding, M., Nicklaus, K., Braxmaier, C., . . . Heinzel, G. (2016).  
888 Laser ranging interferometer on grace follow-on. In B. Cugny, N. Karafolas, & Z. Sodnik  
889 (Eds.), *International conference on space optics - icso 2016* (Vol. 10562). 18.-21-10.2016, Biar-  
890 ritz, France. doi: 10.1117/12.2297705
- 891 Dickerson, S. M., Hogan, J. M., Sugarbaker, A., Johnson, D. M. S., & Kasevich, M. A. (2013). Mul-  
892 ti-axis Inertial Sensing with Long-Time Point Source Atom Interferometry. *Phys. Rev. Lett.*,  
893 *111*(8), 083001. doi: 10.1103/PhysRevLett.111.083001
- 894 Dirx, D., Gurvits, L. I., Lainey, V., Lari, G., Milani, A., Cimò, G., . . . Visser, P. (2017). On the  
895 contribution of pride-juice to jovian system ephemerides. *Planetary and Space Science*, *147*,  
896 14–27. doi: 10.1016/j.pss.2017.09.004
- 897 Dirx, D., Prochazka, I., Bauer, S., Visser, P., Noomen, R., Gurvits, L. I., & Vermeersen, B. (2019).  
898 Laser and radio tracking for planetary science missions—a comparison. *Journal of Geodesy*,  
899 *93*(11), 2405–2420. doi: 10.1007/s00190-018-1171-x
- 900 Dirx, D., Vermeersen, L., Noomen, R., & Visser, P. (2014). Phobos laser ranging: numerical  
901 geodesy experiments for martian system science. *Planetary and Space Science*, *99*, 84–102. doi:  
902 10.1016/j.pss.2014.03.022
- 903 Doo, W.-B., Hsu, S.-K., Lo, C.-L., Chen, S.-C., Tsai, C.-H., Lin, J.-Y., . . . Ma, Y.-F. (2015, Decem-  
904 ber). Gravity anomalies of the active mud diapirs off southwest Taiwan. *Geophysical Journal*  
905 *International*, *203*(3), 2089–2098. doi: 10.1093/gji/ggv430
- 906 Doornbos, E. (2012). *Thermospheric density and wind determination from satellite dynamics* (Doc-  
907 toral dissertation, Delft university of Technology). doi: 10.1007/978-3-642-25129-0
- 908 Douch, K., Wu, H., Schubert, C., Müller, J., & Pereira dos Santos, F. (2018). Simulation-based eval-  
909 uation of a cold atom interferometry gradiometer concept for gravity field recovery. *Advances*

- 910 *in Space Research*, 61(5), 1307–1323. doi: 10.1016/j.asr.2017.12.005
- 911 Dundas, C. M., Mellon, M. T., Conway, S. J., Daubar, I. J., Williams, K. E., Ojha, L., . . . Pathare,  
912 A. V. (2021, March). Widespread Exposures of Extensive Clean Shallow Ice in the  
913 Midlatitudes of Mars. *Journal of Geophysical Research (Planets)*, 126(3), e06617. doi:  
914 10.1029/2020JE006617
- 915 Döringshoff, K., Schuldt, T., Kovalchuk, E. V., Stühler, J., Braxmaier, C., & Peters, A. (2017). A  
916 flight-like absolute optical frequency reference based on iodine for laser systems at 1064 nm.  
917 *Applied Physics B*, 123(6), 183. doi: 10.1007/s00340-017-6756-1
- 918 Efroimsky, M., & Lainey, V. (2007). Physics of bodily tides in terrestrial planets and the appropriate  
919 scales of dynamical evolution. *Journal of Geophysical Research: Planets*, 112, E12003. doi: 10  
920 .1029/2007JE002908
- 921 Fernández Barranco, G., Sheard, B. S., Dahl, C., Mathis, W., & Heinzl, G. (2018). A low-power,  
922 low-noise 37-mhz photoreceiver for intersatellite laser interferometers using discrete heterojunc-  
923 tion bipolar transistors. *IEEE Sensors Journal*, 18(18). doi: 10.1109/JSEN.2018.2857202
- 924 Folkner, W. M., Dehant, V., Le Maistre, S., Yseboodt, M., Rivoldini, A., Van Hoolst, T., . . .  
925 Golombek, M. P. (2018). The rotation and interior structure experiment on the insight mission  
926 to mars. *Space Science Reviews*, 214(5), 100. doi: 10.1007/s11214-018-0530-5
- 927 Freier, C., Hauth, M., Schkolnik, V., Leykauf, B., Schilling, M., Wziontek, H., . . . Peters, A. (2016).  
928 Mobile quantum gravity sensor with unprecedented stability. *Journal of Physics: Conference*  
929 *Series*, 723, 012050. doi: 10.1088/1742-6596/723/1/012050
- 930 Frey, H. V., Roark, J. H., Shockey, K. M., Frey, E. L., & Sakimoto, S. E. H. (2002). Ancient low-  
931 lands on mars. *Geophysical Research Letters*, 29(10), 1384. doi: 10.1029/2001GL013832
- 932 Fryer, P., Wheat, C. G., Williams, T., Kelley, C., Johnson, K., Ryan, J., . . . Pomponi, S. (2020,  
933 February). Mariana serpentinite mud volcanism exhumes subducted seamount materials: impli-  
934 cations for the origin of life. *Philosophical Transactions of the Royal Society of London Series*  
935 *A*, 378(2165), 20180425. doi: 10.1098/rsta.2018.0425
- 936 Gaaloul, N., Meister, M., Corgier, R., Pichery, A., Boegel, P., Herr, W., . . . Bigelow, N. P. (2022). A  
937 space-based quantum gas laboratory at picokelvin energy scales. *arXiv preprint*. doi: 10.48550/  
938 ARXIV.2201.06919
- 939 Geiger, R., Ménoret, V., Stern, G., Zahzam, N., Cheinet, P., Battelier, B., . . . others (2011). Detect-  
940 ing inertial effects with airborne matter-wave interferometry. *Nature communications*, 2, 474.

- 941           doi: 10.1038/ncomms1479
- 942 Genova, A. (2020, January). ORACLE: A mission concept to study Mars' climate, surface and inte-  
 943 rior. *Acta Astronautica*, *166*, 317-329. doi: 10.1016/j.actaastro.2019.10.006
- 944 Genova, A., Goossens, S., Lemoine, F. G., Mazarico, E., Neumann, G. A., Smith, D. E., & Zuber,  
 945 M. T. (2016). Seasonal and static gravity field of mars from mgs, mars odyssey and mro radio  
 946 science. *Icarus*, *272*, 228-245. doi: 10.1016/j.icarus.2016.02.050
- 947 Glassmeier, K.-H. (2020). Solar system exploration via comparative planetology. *Nature Communica-*  
 948 *tions*, *11*(1), 474. doi: 10.1038/s41467-020-18126-z
- 949 Goossens, S., Sabaka, T. J., Genova, A., Mazarico, E., Nicholas, J. B., & Neumann, G. A. (2017).  
 950 Evidence for a low bulk crustal density for mars from gravity and topography. *Geophysical*  
 951 *Research Letters*, *44*(15), 7686-7694. doi: 10.1002/2017GL074172
- 952 Goossens, S., Sabaka, T. J., Wiczorek, M. A., Neumann, G. A., Mazarico, E., Lemoine, F. G., ...  
 953 Zuber, M. T. (2020). High-resolution gravity field models from GRAIL data and implica-  
 954 tions for models of the density structure of the Moon's crust. *Journal of Geophysical Research:*  
 955 *Planets*, *125*(2). doi: 10.1029/2019JE006086
- 956 Goswami, S., Francis, S. P., Bandikova, T., & Spero, R. E. (2021). Analysis of GRACE Follow-  
 957 On Laser Ranging Interferometer derived inter-satellite pointing angles. *IEEE Sensors Journal*,  
 958 *21*(17), 19209-19221. doi: 10.1109/JSEN.2021.3090790
- 959 Grimm, R. E., Harrison, K. P., Stillman, D. E., & Kirchoff, M. R. (2017, January). On the secular  
 960 retention of ground water and ice on Mars. *Journal of Geophysical Research (Planets)*, *122*(1),  
 961 94-109. doi: 10.1002/2016JE005132
- 962 Haagmans, R., Siemes, C., Massotti, L., Carraz, O., & Silvestrin, P. (2020). ESA's next-generation  
 963 gravity mission concepts. *Rend Lincei-Sci Fis*, *31*, 15-25. doi: 10.1007/s12210-020-00875-0
- 964 Haberle, M. R., & Kahre, M. A. (2010). Detecting secular climate change on mars. *The International*  
 965 *Journal of Mars Science and Exploration*, *5*, 68-75. doi: doi:10.1555/mars.2010.0003
- 966 Heinzl, G., Esteban, J. J., Barke, S., Markus, O., Wang, Y., Garcia, A. F., & Danzmann, K. (2011).  
 967 Auxiliary functions of the lisa laser link: ranging, clock noise transfer and data communication.  
 968 *Classical and Quantum Gravity*, *28*(9), 094008. doi: 10.1088/0264-9381/28/9/094008
- 969 Highsmith, D., You, T.-H., Demcak, S., Graat, E., Higa, E., Long, S., ... Peralta, F. (2008). Mars  
 970 reconnaissance orbiter navigation during the primary science phase. In *AIAA/AAS Astro-*  
 971 *dynamics Specialist Conference, 18.-21.08.2008, Honolulu, Hawaii, USA* (p. 092407). doi:

- 972 10.2514/6.2008-6422
- 973 Holt, J. W., Safaeinili, A., Plaut, J. J., Head, J. W., Phillips, R. J., Seu, R., ... Gim, Y. (2008,  
974 November). Radar Sounding Evidence for Buried Glaciers in the Southern Mid-Latitudes of  
975 Mars. *Science*, *322*(5905), 1235. doi: 10.1126/science.1164246
- 976 Hu, Z.-K., Sun, B.-L., Duan, X.-C., Zhou, M.-K., Chen, L.-L., Zhan, S., ... Luo, J. (2013, 10).  
977 Demonstration of an ultrahigh-sensitivity atom-interferometry absolute gravimeter. *Phys. Rev.*  
978 *A*, *88*, 043610. doi: 10.1103/PhysRevA.88.043610
- 979 Iess, L., Asmar, S. W., Cappuccio, P., Cascioli, G., de Marchi, F., Di Stefano, I., ... Zannoni, M.  
980 (2021). Gravity, geodesy and fundamental physics with BepiColombo's MORE investigation.  
981 *Space Science Reviews*, *217*(1), 1–39. doi: 10.1007/s11214-021-00800-3
- 982 Jacobstein, N. (2021). Nasa's perseverance: Robot laboratory on mars. *Science Robotics*, *6*(52),  
983 eabh3167. doi: 10.1126/scirobotics.abh3167
- 984 Jakosky, B. M. (2021). Atmospheric Loss to Space and the History of Water on Mars. *Annual Re-*  
985 *view of Earth and Planetary Sciences*, *49*. doi: 10.1146/annurev-earth-062420-052845
- 986 Karatekin, Ö., de Viron, O., Lambert, S., Dehant, V., Rosenblatt, P., Van Hoolst, T., & Le Maistre,  
987 S. (2011). Atmospheric angular momentum variations of Earth, Mars and Venus at seasonal  
988 time scales. *Planetary and Space Science*, *59*(10), 923-933. doi: 10.1016/j.pss.2010.09.010
- 989 Karatekin, Ö., Duron, J., Rosenblatt, P., Van Hoolst, T., Dehant, V., & Barriot, J. P. (2005). Mars'  
990 time-variable gravity and its determination: Simulated geodesy experiments. *Journal of Geo-*  
991 *physical Research (Planets)*, *110*(E6), E06001. doi: 10.1029/2004JE002378
- 992 Karatekin, Ö., Van Hoolst, T., & Dehant, V. (2006). Martian global-scale CO<sub>2</sub> exchange from time-  
993 variable gravity measurements. *Journal of Geophysical Research (Planets)*, *111*(E6), E06003.  
994 doi: 10.1029/2005JE002591
- 995 Karatekin, Ö., Van Hoolst, T., Tastet, J., de Viron, O., & Dehant, V. (2006). The effects of sea-  
996 sonal mass redistribution and interior structure on Length-of-Day variations of Mars. *Advances*  
997 *in Space Research*, *38*(4), 739-744. doi: 10.1016/j.asr.2005.03.117
- 998 Kasevich, M., & Chu, S. (1991). Atomic interferometry using stimulated Raman transitions. *Phys.*  
999 *Rev. Lett.*, *67*(2), 181–184. doi: 10.1103/PhysRevLett.67.181
- 1000 Kayali, S., Morton, P., & Gross, M. (2017). International challenges of GRACE follow-on. In  
1001 *2017 IEEE Aerospace Conference, 04.-11.03.2007, Big Sky, MT, USA* (pp. 1–8). IEEE. doi: 10  
1002 .1109/AERO.2017.7943615

- 1003 Klimczak, C., Kling, C. L., & Byrne, P. K. (2018). Topographic expressions of large thrust  
1004 faults on mars. *Journal of Geophysical Research: Planets*, *123*(8), 1973-1995. doi:  
1005 10.1029/2017JE005448
- 1006 Klinger, B., & Mayer-Gürr, T. (2016). The role of accelerometer data calibration within grace grav-  
1007 ity field recovery: Results from itsg-grace2016. *Advances in Space Research*, *58*(9), 1597-1609.  
1008 doi: 10.1016/j.asr.2016.08.007
- 1009 Knapmeyer-Endrun, B., Panning, M. P., Bissig, F., Joshi, R., Khan, A., Kim, D., . . . Banerdt, W. B.  
1010 (2021). Thickness and structure of the martian crust from InSight seismic data. *Science*,  
1011 *373*(6553), 438-443. doi: 10.1126/science.abf8966
- 1012 Koch, A. (2020). *Link acquisition and optimization for intersatellite laser interferometry* (Doctoral  
1013 dissertation, Leibniz Universität Hannover). doi: 10.15488/9799
- 1014 Koch, A., Sanjuan, J., Gohlke, M., Mahrtdt, C., Brause, N., Braxmaier, C., & Heinzl, G. (2018).  
1015 Line of sight calibration for the laser ranging interferometer on-board the grace follow-on  
1016 mission: on-ground experimental validation. *Optics Express*, *26*(20), 25892-25908. doi:  
1017 10.1364/OE.26.025892
- 1018 Komatsu, G., Okubo, C. H., Wray, J. J., Ojha, L., Cardinale, M., Murana, A., . . . Gallagher, R.  
1019 (2016). Small edifice features in Chryse Planitia, Mars: Assessment of a mud volcano hypothe-  
1020 sis. *Icarus*, *268*, 56-75. doi: 10.1016/j.icarus.2015.12.032
- 1021 Konopliv, A. S., Asmar, S. W., Folkner, W. M., Karatekin, Ö., Nunes, D. C., Smrekar, S. E., . . .  
1022 Zuber, M. T. (2011). Mars high resolution gravity fields from mro, mars seasonal gravity, and  
1023 other dynamical parameters. *Icarus*, *211*(1), 401-428. doi: 10.1016/j.icarus.2010.10.004
- 1024 Konopliv, A. S., Park, R. S., & Folkner, W. M. (2016). An improved jpl mars gravity field and orien-  
1025 tation from mars orbiter and lander tracking data. *Icarus*, *274*, 253-260. doi: 10.1016/j.icarus  
1026 .2016.02.052
- 1027 Konopliv, A. S., Park, R. S., Rivoldini, A., Baland, R.-M., Le Maistre, S., van Hoolst, T., . . . De-  
1028 hant, V. (2020). Detection of the chandler wobble of mars from orbiting spacecraft. *Geophysical*  
1029 *Research Letters*, *47*(21). doi: 10.1029/2020GL090568
- 1030 Konopliv, A. S., Yoder, C. F., Standish, E. M., Yuan, D.-N., & Sjogren, W. L. (2006). A global  
1031 solution for the mars static and seasonal gravity, mars orientation, phobos and deimos masses,  
1032 and mars ephemeris. *Icarus*, *182*(1), 23-50. doi: 10.1016/j.icarus.2005.12.025
- 1033 Kornfeld, R. P., Arnold, B. W., Gross, M. A., Dahya, N. T., Klipstein, W. M., Gath, P. F., & Bet-

- 1034 tadpur, S. (2019). GRACE-FO: The Gravity Recovery and Climate Experiment Follow-On  
 1035 Mission. *Journal of Spacecraft and Rockets*, *56*(3), 931–951. doi: 10.2514/1.A34326
- 1036 Kuchynka, P., Folkner, W. M., Konopliv, A. S., Parker, T. J., Park, R. S., Le Maistre, S., & Dehant,  
 1037 V. (2014). New constraints on mars rotation determined from radiometric tracking of the  
 1038 opportunity mars exploration rover. *Icarus*, *229*, 340–347. doi: 10.1016/j.icarus.2013.11.015
- 1039 Lachmann, M. D., Ahlers, H., Becker, D., Dinkelaker, A. N., Grosse, J., Hellmig, O., ... Rasel, E. M.  
 1040 (2021). Ultracold atom interferometry in space. *Nature Communications*, *12*(1), 1317. doi:  
 1041 10.1038/s41467-021-21628-z
- 1042 Lainey, V., Pasewaldt, A., Robert, V., Rosenblatt, P., Jaumann, R., Oberst, J., ... Thuillot, W.  
 1043 (2021). Mars moon ephemerides after 14 years of mars express data. *Astronomy & Astro-*  
 1044 *physics*, *650*, A64. doi: 10.1051/0004-6361/202039406
- 1045 Lan, S.-Y., Kuan, P.-C., Estey, B., Haslinger, P., & Müller, H. (2012). Influence of the coriolis force  
 1046 in atom interferometry. *Phys Rev Lett*, *108*(9), 090402. doi: 10.1103/PhysRevLett.108.090402
- 1047 Lauro, S. E., Pettinelli, E., Caprarelli, G., Guallini, L., Rossi, A. P., Mattei, E., ... Orosei, R. (2021,  
 1048 January). Multiple subglacial water bodies below the south pole of Mars unveiled by new  
 1049 MARSIS data. *Nature Astronomy*, *5*, 63-70. doi: 10.1038/s41550-020-1200-6
- 1050 Lautier, J., Volodimer, L., Hardin, T., Merlet, S., Lours, M., Pereira Dos Santos, F., & Landragin, A.  
 1051 (2014). Hybridizing matter-wave and classical accelerometers. *Applied Physics Letters*, *105*(14),  
 1052 144102. doi: 10.1063/1.4897358
- 1053 Lemoine, F. G., Goossens, S., Sabaka, T. J., Nicholas, J. B., Mazarico, E., Rowlands, D. D., ... Zu-  
 1054 ber, M. T. (2013). High-degree gravity models from grail primary mission data. *Journal of*  
 1055 *Geophysical Research: Planets*, *118*(8), 1676-1698. doi: 10.1002/jgre.20118
- 1056 Lévêque, T., Fallet, C., Lefebve, J., Piquereau, A., Gauguier, A., Battelier, B., ... Santos, F. P. D.  
 1057 (2022). Carioqa: Definition of a quantum pathfinder mission. *arXiv preprint*. doi:  
 1058 10.48550/ARXIV.2211.01215
- 1059 Lévêque, T., Fallet, C., Manda, M., Biancale, R., Lemoine, J. M., Tavidel, S., ... Bouyer, P. (2021).  
 1060 Gravity field mapping using laser-coupled quantum accelerometers in space. *Journal of*  
 1061 *Geodesy*, *95*, 15. doi: 10.1007/s00190-020-01462-9
- 1062 Lognonné, P., Banerdt, W. B., Giardini, D., Pike, W., Christensen, U., Laudet, P., ... others (2019).  
 1063 Seis: Insight’s seismic experiment for internal structure of mars. *Space Science Reviews*,  
 1064 *215*(1), 12. doi: 10.1007/s11214-018-0574-6

- 1065 Louchet-Chauvet, A., Farah, T., Bodart, Q., Clairon, A., Landragin, A., Merlet, S., & Pereira  
 1066 Dos Santos, F. (2011). The influence of transverse motion within an atomic gravimeter.  
 1067 *New J. Phys.*, *13*, 065025. doi: 10.1088/1367-2630/13/6/065025
- 1068 Lowry, A. R., & Zhong, S. (2003). Surface versus internal loading of the tharsis rise, mars. *Journal of*  
 1069 *Geophysical Research: Planets*, *108*(E9), 5099. doi: 10.1029/2003JE002111
- 1070 Manda, M., Dehant, V., & Cazenave, A. (2020). GRACE-gravity data for understanding the deep  
 1071 Earth's interior. *Remote Sens*, *12*(24), 4186. doi: 10.3390/rs12244186
- 1072 Mari, N., Hallis, L. J., Daly, L., & Lee, M. R. (2020). Convective activity in a martian magma cham-  
 1073 ber recorded by p-zoning in tissint olivine. *Meteoritics & Planetary Science*, *55*(5), 1057-1072.  
 1074 doi: 10.1111/maps.13488
- 1075 McKenzie, D., Barnett, D. N., & Yuan, D.-N. (2002). The relationship between martian gravity and  
 1076 topography. *Earth and Planetary Science Letters*, *195*(1), 1-16. doi: 10.1016/S0012-821X(01)  
 1077 00555-6
- 1078 Meister, J., Bremer, S., HosseiniArani, A., Leipner, A., List, M., Müller, J., & Schilling, M. (2022).  
 1079 Reference mirror misalignment of cold atom interferometers on satellite-based gravimetry mis-  
 1080 sions. In *73rd International Astronautical Congress (IAC), 18-22 September 2022, Paris,*  
 1081 *France.*
- 1082 Ménoret, V., Vermeulen, P., Le Moigne, N., Bonvalot, S., Bouyer, P., Landragin, A., & Desruelle, B.  
 1083 (2018). Gravity measurements below  $10^{-9}$  g with a transportable absolute quantum gravime-  
 1084 ter. *Scientific Reports*, *8*(1), 12300. doi: 10.1038/s41598-018-30608-1
- 1085 Métivier, L., Karatekin, Ö., & Dehant, V. (2008, April). The effect of the internal structure of Mars  
 1086 on its seasonal loading deformations. *Icarus*, *194*(2), 476-486. doi: 10.1016/j.icarus.2007.12  
 1087 .001
- 1088 Michalski, J. R., Cuadros, J., Niles, P. B., Parnell, J., Deanne Rogers, A., & Wright, S. P. (2013).  
 1089 Groundwater activity on mars and implications for a deep biosphere. *Nature Geoscience*, *6*(2),  
 1090 133-138. doi: 10.1038/ngeo1706
- 1091 Migliaccio, F., Batsukh, K., Benciolini, G. B., Braitenberg, C., Koç, Ö., Mottini, S., ... Vitti, A.  
 1092 (2022). Results of the mocast+ study on a quantum gravimetry mission. In *EGU General*  
 1093 *Assembly, 23.-27.05.2022, Vienna, Austria.* doi: 10.5194/egusphere-egu22-9568
- 1094 Migliaccio, F., Reguzzoni, M., Batsukh, K., Tino, G. M., Rosi, G., Sorrentino, F., ... Zoffoli,  
 1095 S. (2019). Mocass: A satellite mission concept using cold atom interferometry for mea-

- 1096 suring the Earth gravity field. *Surveys in Geophysics*, 40(5), 1029–1053. doi: 10.1007/  
 1097 s10712-019-09566-4
- 1098 Muirhead, B. K., Nicholas, A. K., Umland, J., Sutherland, O., & Vijendran, S. (2020). Mars sam-  
 1099 ple return campaign concept status. *Acta Astronautica*, 176, 131–138. doi: 10.1016/j.actaastro  
 1100 .2020.06.026
- 1101 Müller, V., Hauk, M., Misfeldt, M., Müller, L., Wegener, H., Yan, Y., & Heinzl, G. (2022). Com-  
 1102 paring grace-fo kbr and lri ranging data with focus on carrier frequency variations. *arXiv*  
 1103 *Preprint*.
- 1104 Müntinga, H., Ahlers, H., Krutzik, M., Wenzlawski, A., Arnold, S., Becker, D., ... Rasel, E. M.  
 1105 (2013). Interferometry with Bose-Einstein Condensates in Microgravity. *Phys. Rev. Lett.*, 110,  
 1106 093602. doi: 10.1103/PhysRevLett.110.093602
- 1107 Nazari-Sharabian, M., Aghababaei, M., Karakouzian, M., & Karami, M. (2020). Water on mars—a  
 1108 literature review. *Galaxies*, 8(2), 40. doi: 10.3390/galaxies8020040
- 1109 Nettleton, L. L. (1979, September). Quantitative analysis of a mud volcano gravity anomaly. *Geo-*  
 1110 *physics*, 44(9), 1518. doi: 10.1190/1.1441022
- 1111 Neumann, G. A., Zuber, M. T., Wieczorek, M. A., McGovern, P. J., Lemoine, F. G., & Smith, D. E.  
 1112 (2004, August). Crustal structure of Mars from gravity and topography. *Journal of Geophysical*  
 1113 *Research (Planets)*, 109(E8), E08002. doi: 10.1029/2004JE002262
- 1114 Oberst, J., Wickhusen, K., Gwinner, K., Hauber, E., Stark, A., Elgner, S., ... Hiesinger, H. (2022).  
 1115 Planetary polar explorer - the case for a next-generation remote sensing mission to low Mars  
 1116 orbit. *Experimental Astronomy*. doi: 10.1007/s10686-021-09820-x
- 1117 Oehler, D. Z., & Allen, C. C. (2010, August). Evidence for pervasive mud volcanism in Acidalia  
 1118 Planitia, Mars. *Icarus*, 208(2), 636-657. doi: 10.1016/j.icarus.2010.03.031
- 1119 Oehler, D. Z., Salvatore, M., Etiope, G., & Allen, C. C. (2021). Focusing the Search for Organic  
 1120 Biosignatures on Mars. In *52nd lunar and planetary science conference* (p. 1353).
- 1121 Orgel, C., Hauber, E., van Gasselt, S., Reiss, D., Johnsson, A., Ramsdale, J. D., ... Teodoro,  
 1122 L. F. A. (2019, February). Grid Mapping the Northern Plains of Mars: A New Overview of  
 1123 Recent Water- and Ice-Related Landforms in Acidalia Planitia. *Journal of Geophysical Re-*  
 1124 *search (Planets)*, 124(2), 454-482. doi: 10.1029/2018JE005664
- 1125 O'Rourke, L., Heinisch, P., Blum, J., Fornasier, S., Filacchione, G., Van Hoang, H., ... others  
 1126 (2020). The philae lander reveals low-strength primitive ice inside cometary boulders. *Na-*

- 1127 *ture*, 586(7831), 697–701. doi: 10.1038/s41586-020-2834-3
- 1128 Pail, R., Bingham, R., Braitenberg, C., Dobsław, H., Eicker, A., Güntner, A., . . . IUGG Expert  
1129 Panel (2015). Science and user needs for observing global mass transport to understand global  
1130 change and to benefit society. *Surv Geophys*, 36(6), 743–772. doi: 10.1007/s10712-015-9348-9
- 1131 Peddinti, D. A., & McNamara, A. K. (2019). Dynamical investigation of a thickening ice-shell: Impli-  
1132 cations for the icy moon europa. *Icarus*, 329, 251–269. doi: 10.1016/j.icarus.2019.03.037
- 1133 Peters, A., Chung, K. Y., & Chu, S. (1999). Measurement of gravitational acceleration by dropping  
1134 atoms. *Nature*, 400, 849–852. doi: 10.1038/23655
- 1135 Petricca, F., Genova, A., Goossens, S., Iess, L., & Spada, G. (2022). Constraining the internal struc-  
1136 tures of venus and mars from the gravity response to atmospheric loading. *The Planetary Sci-*  
1137 *ence Journal*, 3(7), 164. doi: 10.3847/PSJ/ac7878
- 1138 Phillips, R. J., Zuber, M. T., Solomon, S. C., Golombek, M. P., Jakosky, B. M., Banerdt, W. B.,  
1139 . . . II, S. A. H. (2001). Ancient geodynamics and global-scale hydrology on mars. *Science*,  
1140 291(5513), 2587–2591. doi: 10.1126/science.1058701
- 1141 Pou, L., Nimmo, F., Rivoldini, A., Khan, A., Bagheri, A., Gray, T., . . . others (2022). Tidal  
1142 constraints on the martian interior. *Journal of Geophysical Research: Planets*, 127(11),  
1143 e2022JE007291. doi: 10.1029/2022JE007291
- 1144 Rakholia, A. V., McGuinness, H. J., & Biedermann, G. W. (2014). Dual-axis high-data-rate atom  
1145 interferometer via cold ensemble exchange. *Phys. Rev. Applied*, 2(5), 054012. doi: 10.1103/  
1146 PhysRevApplied.2.054012
- 1147 Rees, E. R., Wade, A. R., Sutton, A. J., & McKenzie, K. (2022). Absolute frequency readout of cav-  
1148 ity against atomic reference. *Remote Sensing*, 14(11), 2689. doi: 10.3390/rs14112689
- 1149 Rees, E. R., Wade, A. R., Sutton, A. J., Spero, R. E., Shaddock, D. A., & McKenzie, K. (2021). Ab-  
1150 solute frequency readout derived from ule cavity for next generation geodesy missions. *Optics*  
1151 *Express*, 29(16), 26014–26027. doi: 10.1364/OE.434483
- 1152 Richardson, L. L., Rajagopalan, A., Albers, H., Meiners, C., Nath, D., Schubert, C., . . . Guzmán, F.  
1153 (2020). Optomechanical resonator-enhanced atom interferometry. *Communications Physics*,  
1154 3(1), 208. doi: 10.1038/s42005-020-00473-4
- 1155 Rivoldini, A., Van Hoolst, T., Verhoeven, O., Mocquet, A., & Dehant, V. (2011). Geodesy con-  
1156 straints on the interior structure and composition of mars. *Icarus*, 213(2), 451–472. doi: 10  
1157 .1016/j.icarus.2011.03.024

- 1158 Root, B., Fulla, J., Ebbing, J., & Martinec, Z. (2021). Combining the deep Earth and lithospheric  
1159 gravity field to study the density structure of the upper mantle. In *EGU General Assembly,*  
1160 *19.-30.04.2021, Vienna, Austria.* doi: 10.5194/egusphere-egu21-2950
- 1161 Root, B., Novák, P., Dirkx, D., Kaban, M., van der Wal, W., & Vermeersen, L. (2016). On a spectral  
1162 method for forward gravity field modelling. *Journal of Geodynamics, 97,* 22-30. doi: 10.1016/j  
1163 .jog.2016.02.008
- 1164 Root, B., & Qin, W. (2022). A re-analysis of the lithospheric flexure on mars. In *Europlanet Science*  
1165 *Congress 2022, 18.-23.09.2022, Granada, Spain* (Vol. 16). doi: 10.5194/epsc2022-375
- 1166 Root, B. C., Sebera, J., Szwillus, W., Thieulot, C., Martinec, Z., & Fulla, J. (2022). Benchmark for-  
1167 ward gravity schemes: the gravity field of a realistic lithosphere model winterc-g. *Solid Earth,*  
1168 *13*(5), 849–873. doi: 10.5194/se-13-849-2022
- 1169 Root, B. C., van der Wal, W., Novák, P., Ebbing, J., & Vermeersen, L. L. A. (2015). Glacial iso-  
1170 static adjustment in the static gravity field of fennoscandia. *Journal of Geophysical Research:*  
1171 *Solid Earth, 120*(1), 503-518. doi: 10.1002/2014JB011508
- 1172 Rosen, M. D. (2021). *Analysis of hybrid satellite-to-satellite tracking and quantum gravity gra-*  
1173 *diometry architecture for time-variable gravity sensing missions* (Doctoral dissertation, The  
1174 University of Texas at Austin). doi: 10.26153/tsw/14541
- 1175 Rudolph, J., Herr, W., Grzeschik, C., Sternke, T., Grote, A., Popp, M., ... Peters, A. (2015). A  
1176 high-flux bec source for mobile atom interferometers. *New J. Phys., 17,* 065001. doi: 10.1088/  
1177 1367-2630/17/6/065001
- 1178 Rummel, R., Yi, W., & Stummer, C. (2011). Goce gravitational gradiometry. *Journal of Geodesy,*  
1179 *85,* 777-790. doi: 10.1007/s00190-011-0500-0
- 1180 Sanjuan, J., Abich, K., Gohlke, M., Resch, A., Schuldt, T., Wegehaupt, T., ... Braxmaier, C. (2019).  
1181 Long-term stable optical cavity for special relativity tests in space. *Optics express, 27*(25),  
1182 36206–36220. doi: 10.1364/OE.27.036206
- 1183 Savoie, D., Altorio, M., Fang, B., Sidorenkov, L. A., Geiger, R., & Landragin, A. (2018). Interleaved  
1184 atom interferometry for high-sensitivity inertial measurements. *Science Advances, 4.* doi: 10  
1185 .1126/sciadv.aau7948
- 1186 Schütze, D., Stede, G., Müller, V., Gerberding, O., Bandikova, T., Sheard, B. S., ... Danzmann,  
1187 K. (2014). Laser beam steering for GRACE Follow-On intersatellite interferometry. *Optics*  
1188 *Express, 22*(20), 24117–24132. doi: 10.1364/OE.22.024117

- 1189 Skinner, J. A., & Tanaka, K. L. (2007, January). Evidence for and implications of sedimentary  
1190 diapirism and mud volcanism in the southern Utopia highland lowland boundary plain, Mars.  
1191 *Icarus*, *186*(1), 41-59. doi: 10.1016/j.icarus.2006.08.013
- 1192 Smith, D. E., Zuber, M. T., & Neumann, G. A. (2001, December). Seasonal Variations of Snow  
1193 Depth on Mars. *Science*, *294*(5549), 2141-2146. doi: 10.1126/science.1066556
- 1194 Smith, I. B., Lalich, D. E., Rezza, C., Horgan, B. H. N., Whitten, J. L., Nerozzi, S., & Holt, J. W.  
1195 (2021, August). A Solid Interpretation of Bright Radar Reflectors Under the Mars South Polar  
1196 Ice. *Geophysical Research Letters*, *48*(15), e93618. doi: 10.1029/2021GL093618
- 1197 Smith, M. D. (2009). Themis observations of mars aerosol optical depth from 2002–2008. *Icarus*,  
1198 *202*(2), 444-452. doi: 10.1016/j.icarus.2009.03.027
- 1199 Stähler, S. C., Khan, A., Banerdt, W. B., Lognonné, P., Giardini, D., Ceylan, S., ... Smrekar,  
1200 S. E. (2021, July). Seismic detection of the martian core. *Science*, *373*(6553), 443-448. doi:  
1201 10.1126/science.abi7730
- 1202 Stamenkovic, V., Lynch, K., Boston, P., Tarnas, J., Edwards, C. D., Sherwood-Lollar, B., ... Timo-  
1203 ney, R. (2021, May). Deep Trek: Science of Subsurface Habitability & Life on Mars. In *Bulletin*  
1204 *of the american astronomical society* (Vol. 53, p. 250). doi: 10.3847/25c2cfcb.dc18f731
- 1205 Starichenko, E. D., Belyaev, D. A., Medvedev, A. S., Fedorova, A. A., Korablev, O. I., Trokhi-  
1206 movskiy, A., ... Hartogh, P. (2021). Gravity wave activity in the martian atmosphere at  
1207 altitudes 20–160 km from acs/tgo occultation measurements. *Journal of Geophysical Research:*  
1208 *Planets*, *126*(8), e2021JE006899. doi: 10.1029/2021JE006899
- 1209 Steffen, H., Gitlein, O., Denker, H., Müller, J., & Timmen, L. (2009). Present rate of uplift in  
1210 Fennoscandia from GRACE and absolute gravimetry. *Tectonophysics*, *474*(1-2), 69–77. doi:  
1211 10.1016/j.tecto.2009.01.012
- 1212 Sutton, A., McKenzie, K., Ware, B., & Shaddock, D. A. (2010). Laser ranging and communications  
1213 for lisa. *Optics express*, *18*(20), 20759-20773. doi: 10.1364/OE.18.020759
- 1214 Tapley, B. D., Bettadpur, S., Ries, J. C., Thompson, P. F., & Watkins, M. M. (2004). GRACE Mea-  
1215 surements of Mass Variability in the Earth System. *Science*, *305*(5683), 503–505. doi: 10.1126/  
1216 science.1099192
- 1217 Tapley, B. D., Watkins, M. M., Flechtner, F., Reigber, C., Bettadpur, S., Rodell, M., ... Velicogna,  
1218 I. (2019). Contributions of GRACE to understanding climate change. *Nat Clim Change*, *9*(5),  
1219 358–369. doi: 10.1038/s41558-019-0456-2

- 1220 Thompson, R., Folkner, W. M., deVine, G., Klipstein, W. M., McKenzie, K., Spero, R., . . . Shad-  
 1221 dock, D. A. (2011). A flight-like optical reference cavity for grace follow-on laser frequency  
 1222 stabilization. In *2011 Joint Conference of the IEEE International Frequency Control and the*  
 1223 *European Frequency and Time Forum (FCS) Proceedings, 02.-05.05.2011, San Francisco, Tx,*  
 1224 *USA* (Vol. 10562). doi: 10.1109/FCS.2011.5977873
- 1225 Touboul, P., Foulon, B., Christophe, B., & Marque, J. P. (2012). Champ, grace, goce instru-  
 1226 ments and beyond. In S. Kenyon, M. C. Pacino, & U. Marti (Eds.), *Geodesy for planet*  
 1227 *earth* (Vol. 136, pp. 215–221). Berlin, Heidelberg: Springer Berlin Heidelberg. doi:  
 1228 10.1007/978-3-642-20338-1\_26
- 1229 Trimeche, A., Battelier, B., Becker, D., Bertoldi, A., Bouyer, P., Braxmaier, C., . . . Pereira dos  
 1230 Santos, F. (2019). Concept study and preliminary design of a cold atom interferome-  
 1231 ter for space gravity gradiometry. *Classical and Quantum Gravity*, *36*(21), 215004. doi:  
 1232 10.1088/1361-6382/ab4548
- 1233 Turcotte, D. L., Willemann, R. J., Haxby, W. F., & Norberry, J. (1981). Role of membrane stresses  
 1234 in the support of planetary topography. *Journal of Geophysical Research: Solid Earth*, *86*(B5),  
 1235 3951-3959. doi: 10.1029/JB086iB05p03951
- 1236 van Zoest, T., Gaaloul, N., Singh, Y., Ahlers, H., Herr, W., Seidel, S. T., . . . Reichel, J. (2010).  
 1237 Bose-Einstein Condensation in Microgravity. *Science*, *328*, 1540-1543. doi: 10.1126/  
 1238 science.1189164
- 1239 van Brummen, B. (2022). *Mars gravity inversion: Investigating the lateral density variations of the*  
 1240 *martian lithosphere* (Master's Thesis, Delft University of Technology). Retrieved from [http://](http://resolver.tudelft.nl/uuid:1f8beaf8-a97a-47d5-a57b-38b91a35bec9)  
 1241 [resolver.tudelft.nl/uuid:1f8beaf8-a97a-47d5-a57b-38b91a35bec9](http://resolver.tudelft.nl/uuid:1f8beaf8-a97a-47d5-a57b-38b91a35bec9)
- 1242 Watts, A., & Burov, E. (2003). Lithospheric strength and its relationship to the elastic and seis-  
 1243 mogenic layer thickness. *Earth and Planetary Science Letters*, *213*(1), 113-131. doi: 10.1016/  
 1244 S0012-821X(03)00289-9
- 1245 Wiczorek, M. A., Broquet, A., McLennan, S. M., Rivoldini, A., Golombek, M., Antonangeli,  
 1246 D., . . . Banerdt, W. B. (2022, May). InSight Constraints on the Global Character of  
 1247 the Martian Crust. *Journal of Geophysical Research (Planets)*, *127*(5), e07298. doi:  
 1248 10.1029/2022JE007298
- 1249 Williams, J. G., Konopliv, A. S., Boggs, D. H., Park, R. S., Yuan, D.-N., Lemoine, F. G., . . . others  
 1250 (2014). Lunar interior properties from the grail mission. *Journal of Geophysical Research:*

- 1251 *Planets*, 119(7), 1546–1578. doi: 10.1002/2013JE004559
- 1252 Xiao, H., Stark, A., Schmidt, F., Hao, J., Steinbrügge, G., Wagner, N. L., ... Oberst, J. (2022).  
 1253 Spatio-temporal level variations of the martian seasonal north polar cap from co-registration of  
 1254 mola profiles. *Journal of Geophysical Research: Planets*, 127(10). doi: 10.1029/2021JE007158
- 1255 Xiao, H., Stark, A., Schmidt, F., Hao, J., Su, S., Steinbrügge, G., & Oberst, J. (2022). Spatio-  
 1256 temporal level variations of the martian seasonal south polar cap from co-registration of mola  
 1257 profiles. *Journal of Geophysical Research: Planets*, 127(7). doi: 10.1029/2022JE007196
- 1258 Yoder, C. F., Konopliv, A. S., Yuan, D. N., Standish, E. M., & Folkner, W. M. (2003). Fluid core  
 1259 size of mars from detection of the solar tide. *Science*, 300(5617), 299-303. doi: 10.1126/science  
 1260 .1079645
- 1261 Zahzam, N., Christophe, B., Lebat, V., Hardy, E., Huynh, P.-A., Marquet, N., ... Carraz, O. (2022).  
 1262 Hybrid electrostatic-atomic accelerometer for future space gravity missions. *Remote Sensing*,  
 1263 14(14). doi: 10.3390/rs14143273
- 1264 Zhong, S., & Roberts, J. H. (2003). On the support of the tharsis rise on mars. *Earth and Planetary  
 1265 Science Letters*, 214(1), 1-9. doi: 10.1016/S0012-821X(03)00384-4
- 1266 Zhong, S., Zhang, N., Li, Z.-X., & Roberts, J. H. (2007). Supercontinent cycles, true polar wander,  
 1267 and very long-wavelength mantle convection. *Earth and Planetary Science Letters*, 261(3), 551-  
 1268 564. doi: 10.1016/j.epsl.2007.07.049
- 1269 Zingerle, P., Pail, R., Gruber, T., & Oikonomidou, X. (2020). The combined global gravity field  
 1270 model xgm2019e. *Journal of Geodesy*, 94(7), 66. doi: 10.1007/s00190-020-01398-0
- 1271 Zuber, M. T., Smith, D. E., Watkins, M. M., Asmar, S. W., Konopliv, A. S., Lemoine, F. G., ...  
 1272 others (2013). Gravity field of the moon from the gravity recovery and interior laboratory  
 1273 (grail) mission. *Science*, 339(6120), 668–671. doi: 10.1126/science.1231507
- 1274 Zuber, M. T., Solomon, S. C., Phillips, R. J., Smith, D. E., Tyler, G. L., Aharonson, O., ... Zhong,  
 1275 S. (2000). Internal structure and early thermal evolution of mars from mars global surveyor  
 1276 topography and gravity. *Science*, 287(5459), 1788-1793. doi: 10.1126/science.287.5459.1788
- 1277 Zurek, R. W., Tolson, R. A., Bougher, S. W., Lugo, R. A., Baird, D. T., Bell, J. M., & Jakosky,  
 1278 B. M. (2017, March). Mars thermosphere as seen in MAVEN accelerometer data. *Journal of  
 1279 Geophysical Research (Space Physics)*, 122(3), 3798-3814. doi: 10.1002/2016JA023641